# ABSTRACT


| | |
|---|---|
| Title of Dissertation: | QUANTIFYING EFFECTS OF SEASONAL INUNDATION ON METHANE FLUXES FROM FORESTED FRESHWATER WETLANDS |
| | Kelly Lynn Hondula, Doctor of Philosophy, 2021 |
| Dissertation directed by: | Dr. Margaret Palmer<br>Distinguished University Professor,<br>Department of Entomology and Director,<br>National Socio-Environmental Synthesis Center |

Developing effective strategies for reducing methane and other greenhouse gas emissions requires a quantitative understanding of their global sources and sinks. Decomposition of organic matter in wet soils is one of the largest sources of methane to the atmosphere, but it is a highly variable process that remains difficult to quantify because we lack a predictive understanding of how environmental factors control methane emissions in wetlands. Hydrology is one of the most important factors controlling methane production wetlands along with temperature and vegetation, however it is unclear how to relate aspects of a wetland's hydrologic regime to the timing, magnitude, and spatial extent of its methane emissions. Furthermore, discrepancies between the magnitude of global methane emissions calculated using different techniques indicate that current methods for measuring the extent and

dynamics of wetland areas in global models may not adequately represent processes controlling methane cycling in wetlands and other small water bodies.

I studied the role of seasonal hydrologic variability on methane emissions from forested mineral soil wetlands to inform modeling techniques at different scales. In Chapter 1, I show the importance of inundation extent and duration as major drivers of wetland methane emissions, that methane fluxes have a non-linear relationship with water level, and that methane fluxes are higher when water levels are falling rather than rising. In Chapter 2, I demonstrate a new technique for calculating methane emissions using high resolution satellite data to quantify wetland inundation time series, and some limits of current technology for modeling surface water dynamics in forested wetlands. Chapter 3 presents and applies a modeling framework for quantifying hydrologic fluxes of methane in the context of common forms of wetland restoration

In combination, these studies establish how and why quantifying the hydrologic regime of seasonally inundated forested wetlands enables a more accurate estimation of methane emissions at multiple scales, that water level drawdown associated with the natural hydrologic regime of forested wetlands considerably reduces methane producing areas, and that improved methods for detecting and modeling surface water dynamics in low relief landscapes will improve our ability to quantify methane emissions.

# QUANTIFYING EFFECTS OF SEASONAL INUNDATION ON METHANE FLUXES FROM FORESTED FRESHWATER WETLANDS

by

Kelly Lynn Hondula

Dissertation submitted to the Faculty of the Graduate School of the
University of Maryland, College Park, in partial fulfillment
of the requirements for the degree of
Doctor of Philosophy
2021

Advisory Committee:
Professor Margaret A. Palmer, Chair
Michael Gonsior
Laura Lapham
Karen Prestegaard
Michael R. Williams
Stephanie Yarwood

# Preface

This dissertation comprises an introduction, three research chapters, and a summary and conclusions section. All research chapters are presented in manuscript form. Tables, figures, and captions occur at the conclusion of each chapter. A single literature cited section occurs at the end for references made throughout the entire dissertation.

*When I am among the trees,*
*especially the willows and the honey locust,*
*equally the beech, the oaks and the pines,*
*they give off such hints of gladness.*
*I would almost say that they save me, and daily.*

*I am so distant from the hope of myself,*
*in which I have goodness, and discernment,*
*and never hurry through the world*
*but walk slowly, and bow often.*

*Around me the trees stir in their leaves*
*and call out, "Stay awhile."*
*The light flows from their branches.*

*And they call again, "It's simple," they say,*
*"and you too have come*
*into the world to do this, to go easy, to be filled*
*with light, and to shine."*

*--Mary Oliver*

# Acknowledgements

I am ever grateful to my advisor, Margaret Palmer, as a source of inspiration, mentoring, and for giving me the opportunity to pursue this research. She has endlessly supported my intellectual curiosity and her example has always encouraged and challenged me to think deeper about why and how to pursue science that matters for the benefit of society. I would also like to thank the members of my committee, Michael Gonsior, Laura Lapham, Karen Prestegaard, Michael Williams, and Stephanie Yarwood for their insight and guidance over the years. This research would also not have been possible without Nate Jones and Ben DeVries, who have been incredibly supportive and insightful collaborators.

I am indebted to all the members of the Palmer lab group especially Alec Armstrong, Christine Maietta, Jake Hosen, Graham Stewart, Anna Kottkamp, and Julianna Greenberg, who have provided an enlightening, supportive, and enjoyable environment in the field, lab, office, and remotely. I would also like to thank collaborators who have provided resources, insight, and other support for this project especially Laurie Alexander, Megan Lang, and Greg McCarty, as well as all of the staff and postdocs at SESYNC.

This research was conducted on land that is part of the traditional territory of the Lenapehoking, currently home to the Confederation of Sovereign Nanticoke-Lenape Tribes People, and graciously protected and managed by The Nature Conservancy. This research benefited by funding to the National Socio-Environmental Synthesis

Center from the National Science Foundation DBI-1639145, and through fellowships from the rOpenSci organization and the National Ecological Observatory Network.

Lastly, I would like to thank my family and friends for support, guidance, and inspiration especially my brother David Hondula, my parents Betty and Dave Hondula, as well as the 217 porch and Stefan Ploum for being invaluable lifelines during COVID.

# Table of Contents

# List of Tables

## Chapter 1: Effects of Seasonal Inundation on Methane Fluxes from Forested Freshwater Wetlands



## Chapter 2: Effects of Using High Resolution Satellite-based Inundation Time Series to Estimate Methane Fluxes from Forested Wetlands

# List of Figures

**Chapter 1: Effects of Seasonal Inundation on Methane Fluxes from Forested Freshwater Wetlands**

**Chapter 3: Quantifying Hydrologic Fluxes of Dissolved Methane from Headwater Wetlands**

# Introduction

Methane concentrations in the atmosphere have more than doubled since pre-industrial times, and the previous decade the rate of increase has also risen. In addition to being a precursor for ground-level air pollutants like ozone, methane is considered the second most important greenhouse gas behind carbon dioxide, responsible for almost one quarter of the additional radiative forcing in the lower atmosphere since 1750. Compared to carbon dioxide, methane has a short lifespan in the atmosphere, which means that emissions reductions can result in reduced climate impacts on the order of decades.

Developing effective strategies for reducing methane emissions requires a quantitative understanding of its global sources and sinks, which is currently lacking. Decomposition of organic matter in wet soils is one of the largest sources of methane to the atmosphere, but it is a highly variable process that remains difficult to quantify because we lack a predictive understanding of how environmental factors control methane emissions in wetlands. Hydrology is one of the most important factors controlling methane production wetlands along with temperature and vegetation, however it is unclear how to relate aspects of a wetland's hydrologic regime to the timing, magnitude, and spatial extent of its methane emissions. Furthermore, discrepancies between the magnitude of global methane emissions calculated using different techniques indicate that current methods for measuring the extent and dynamics of wetland areas in global models may not adequately represent processes controlling methane cycling in wetlands and other small water bodies.

For this dissertation, I studied the role of seasonal hydrologic variability on methane emissions from forested mineral soil wetlands in the mid-Atlantic coastal plain on the Delmarva peninsula. I used a combination of field measurements, modeling, and remote sensing analyses to quantify the relationship between wetland hydrologic regime and methane emissions to inform modeling techniques at different scales. Below is a brief description of the material presented in each chapter and the major findings of this research.

**Chapter 1: Effects of Seasonal Inundation on Methane Fluxes from Forested Freshwater Wetlands**

Methane emissions from small freshwater ecosystems represent one of the largest components of uncertainty in the global methane budget. While these systems are known to produce large amounts of methane relative to their size, quantifying the timing, magnitude, and spatial extent of their emissions remains challenging. We begin to address this challenge in seasonally inundated forested mineral soil wetlands by 1) measuring wetland methane fluxes and hydrologic regime across both inundated and non-inundated soils, 2) characterizing how wetland hydrologic regime impacts the spatial extent of methane emission source areas, and 3) modeling average daily wetland-scale flux rates using four different upscaling techniques. Our results show that inundation extent and duration, but not frequency or depth, were major drivers of wetland methane concentrations. Moreover, we found that methane fluxes were best described by the direction of water level change (i.e. rising or falling),

where emissions were generally higher when water levels were falling. Once soils were inundated, subsequent changes in water level did not explain observed variability of methane concentrations in standing water. Finally, our spatial modeling suggests that representing inundation and associated methane source areas is a critical step in estimating local to regional scale methane emissions. Intermittently inundated soils alternated between being sources and sinks of methane depending on water level, soil moisture, and the direction of water level change. These results demonstrate that quantifying the hydrologic regime of seasonally inundated forested freshwater wetlands enables a more accurate estimation of methane emissions.

**Chapter 2: Effects of Using High Resolution Satellite-based Inundation Time Series to Estimate Methane Fluxes from Forested Wetlands**

A major source of uncertainty in the global methane budget arises from quantifying the area of wetlands and other inland waters. This study addresses how the dynamics of surface water extent in forested wetlands affect the calculation of methane emissions. We used fine resolution satellite imagery acquired at sub-weekly intervals together with a semi-empirical methane emissions model to estimate daily surface water extent and diffusive methane fluxes for a low-relief wetland-rich watershed. Comparisons of surface water model predictions to field measurements showed agreement with the magnitude of changes in water extent, including for wetlands with surface area less than 1,000 $m^2$. Results of methane emission models showed that wetlands smaller than 1 hectare (10,000 $m^2$) were responsible for a majority of emissions, and that considering dynamic inundation of forested wetlands resulted in

49–62% lower emission totals compared to models using a single estimate for each wetland's size.

## Chapter 3: Quantifying Hydrologic Fluxes of Dissolved Methane from Headwater Wetlands

Observations of high methane emissions from restored wetlands have raised questions about the net climate benefits of wetland restoration. However current methods for evaluating the tradeoff between carbon storage and greenhouse gas emissions fail to account for hydrologically mediated fluxes such as transport of dissolved methane out wetlands in runoff and drainage channels. Many wetlands have natural or man-made outlets that provide such hydrologic connections to downstream waters at least seasonally or intermittently, through which methane produced in wetland soils can be advected downstream. It is unclear whether the magnitude of these fluxes comprises a substantial portion of a wetland's total methane output. This chapter presents a framework for quantifying this hydrologic flux of dissolved methane as well as its relative importance in a wetland's total methane output. We apply the framework to a headwater wetland catchment located in a landscape affected by drainage for agriculture and demonstrate that the hydrologic flux can comprise a substantial portion of output. Results from an advection model suggest that a large portion of this dissolved methane can be transported to the perennial stream network before evasion to the atmosphere.

# Chapter 1: Effects of seasonal inundation on methane fluxes from forested freshwater wetlands

*Introduction*

Methane emissions from small freshwater ecosystems such as ponds and forested wetlands represent one of the largest components of uncertainty in the global methane budget. Inventory-based estimates of freshwater methane emissions are higher than expected when compared to top-down models based on atmospheric observations (Saunois et al., 2020a). In part, this discrepancy stems from uncertainty in quantifying methane emissions from mineral soil wetlands, and more specifically, identifying source areas of methane fluxes across intermittently inundated soils. Studies show conflicting reports on how water level variability and wet–dry cycles influence methane fluxes, and it is unclear whether intermittently inundated mineral soils are significant sources of methane (Kim et al., 2012; Marcé et al., 2019). While diurnal variability (Sieczko et al., 2020), trophic status (DelSontro et al., 2018b), the spatial representation of wetland areas (Hondula, DeVries, et al., 2021; Zhang et al., 2016), and within-lake heterogeneity (Natchimuthu et al., 2016) may also explain some of the discrepancy, the potential importance of variable wetland inundation is undetermined.

Methane fluxes are highly variable in freshwater ecosystems and environmental controls on production, consumption, and transport are poorly constrained (Hendriks

et al., 2010; Peltola et al., 2015). Variability in wetland hydrologic conditions, or the wetland hydrologic regime, is a dominant control of methane emissions (Altor & Mitsch, 2008; Bartlett & Harriss, 1993) but its effects are difficult to separate from those of temperature, vegetation, and disturbance history because in wetlands these variables can co-vary and have multiple hierarchical and interactive effects (Bhullar et al., 2013; Golladay et al., 2021; Herbst et al., 2011; Pennock et al., 2010; Turetsky et al., 2014; Vanselow-Algan et al., 2015; Waddington & Day, 2007).

Complex and non-linear relationships between hydrologic and biogeochemical processes in wetlands make it challenging to develop predictive relationships between hydrologic variables and wetland-scale methane emissions. The traditional relationship between water table and emissions is based on assumed separation of an anoxic zone of net production (below the water table) from an oxic zone of net consumption (above the water table) (Bridgham et al., 2013). However, numerous complications have been identified that are hard to account for with this simplification. First, production is not limited to below the water table because methanogenesis can occur in anoxic microsites in otherwise oxygenated soil above the water table (Grossart et al., 2011; Keiluweit et al., 2017; Knorr et al., 2009; Yang et al., 2017). Second, methanotrophy is not limited to the oxic portion of the soil column in the presence of anaerobic methane oxidizers (Angle et al., 2017; McNamara et al., 2006). Time series of flux measurements have also shown temporal lags between changes in water level and changes in methane emissions (Chamberlain et al., 2016; Tangen & Bansal, 2019), and lateral concentration gradients caused by

plants can spatially separate areas of production from emissions (Bansal et al., 2020). Finally, in wetlands with surface inundation, transport and reaction processes in surface water can modulate the amount of methane that reaches the atmosphere (Boon & Lee, 1997; Holgerson et al., 2017; Poindexter et al., 2016). Some authors have suggested that deeper surface inundation should result in more methane oxidation because of slow gas diffusion through water (Altor & Mitsch, 2008; Podgrajsek et al., 2014). Although there is often less dissolved methane in deep (> 6 m) compared to shallow water of lakes (Bastviken et al., 2008), this pattern has not been demonstrated for shallower wetlands.

In addition to hydrologic drivers of methane production and consumption, the assumptions about methane cycling in different land cover types may contribute large uncertainty to emission estimates. Land cover classifications of wetlands generally exclude inundated mineral soils (Poulter et al., 2017a). This omission means that flooded areas of mineral soil in forests, which can be locally or intermittently high methane sources (Desai et al., 2015; Lohila et al., 2016; Sakabe et al., 2016; Teh et al., 2014), do not typically register as methane producing areas in models (Hondula, DeVries, et al., 2021). Instead, mineral forest soils are considered the largest terrestrial sink for atmospheric methane (Dutaur & Verchot, 2007). Among the most well-studied type of wetlands—peatlands—methane fluxes are generally negative when the water table drops to ~10 cm below the peat surface (e.g. (Jungkunst & Fiedler, 2007), but it is unclear how intermittent flooding affects methane fluxes in fundamentally different wetland types (Turetsky et al., 2014). The transition between

methane sources and sinks in temperate forested wetlands may be a dynamic zone controlled by soil moisture (Desai et al., 2015; Fest et al., 2017; Lohila et al., 2016); however, no studies have explicitly attempted to quantify how this boundary varies in time or space.

Treating intermittently or seasonally flooded mineral soils as potential sources of even very small methane fluxes has large implications in emission models because of how expansive this area is globally (Bridgham et al., 2006; Grinham et al., 2018a; Pekel et al., 2016a; Spahni et al., 2011). Filling this gap in our understanding of methane emissions is important for informing earth system models that rely on observations of surface water for determining areal extent of emissions (Bohn et al., 2013; Wania et al., 2013). Improved representation of inundation dynamics in forested wetlands for methane emission models is especially warranted given that forested wetlands experienced the largest change in area of any wetland type in the United States between 2004-2009 (Dahl, 2011b), and the area of soils experiencing periodic drying or inundation cycles may be expanding due to increasing variability in precipitation rates and development-induced land cover changes (Kannenberg et al., 2015).

Here, we assessed the role of hydrologic variability on methane emissions in freshwater forested mineral soil wetlands by 1) quantifying the relationship between water level above (+) and below (-) the soil surface and methane flux rates throughout a water year, 2) characterizing the spatial extent of methane emission source areas for

seasonally dynamic wetlands, and 3) comparing wetland-scale flux estimates using different upscaling techniques.

*Methods*

We measured methane fluxes monthly across inundation gradients in six forested wetlands over one water year and quantified the hydrologic regime of each wetland from water levels monitored at multiple points within each wetland. The relationship between water level and methane flux rates, and the extent of methane emission source areas were evaluated with statistical models. Water level time series and average flux rates from inundated and non-inundated zones were used to estimate wetland-scale emissions under contrasting assumptions regarding methane source area dynamics.

### Study area and hydrologic setting

We identified six forested wetlands in the mid-Atlantic Coastal Plain characterized by seasonal changes in water level and minimal emergent vegetation. Sites were in the Upper Choptank River watershed on the Delmarva peninsula which drains to Chesapeake Bay (Figure 1.1). This low-gradient watershed comprises 60% cropland, 20% woody wetland, 12% forest, and <5% developed land (Dewitz, 2019). Forests contain a patchwork of seasonally flooded area, complex microtopography, sphagnum, narrow ditches from a legacy of drainage, and abundant depressional wetlands called Delmarva bays (Fisher et al., 2010a). These features range in size from 0.5–0.7 hectares (Fenstermacher et al., 2014a; Huang et al., 2014a) and include

large open canopy areas as well as more numerous small forested depressions (M. Lang et al., 2012; M. Vanderhoof et al., 2017); the latter of which are the focus for this study. Depressions have a seasonal hydrologic regime driven by evapotranspiration from a highly permeable shallow groundwater aquifer. They are inundated up to ~150 cm above the soil during late fall and winter, then, depending on rainfall and landscape position, may lose all surface water as the regional water table drops throughout the growing season (Phillips & Shedlock, 1993a). Soils at our study sites are poorly or very poorly drained, with either loamy sand, mucky loam, or moderately decomposed plant material comprising the top 5 cm (Table 1.1; (Soil Survey Staff, 2020)).

Methane measurements were made near each wetland center and at five evenly spaced locations along wetland to upland transects (Figure 1.2). This captured both temporal and spatial variations in hydrologic conditions, which we quantified using metrics described below and in Table 1.2. Throughout, water level refers to the position of the wetland water table relative to the soil surface: positive values indicate inundation and negative values indicate soils were not inundated. The broader water table surrounding a wetland is referred to as the groundwater table (Phillips & Shedlock, 1993a). While the timing and seasonality of precipitation and evapotranspiration drive temporal variation in hydrologic conditions (S. Lee et al., 2019), wetland morphometry drives spatial gradients in hydrologic conditions (i.e., both inundation duration and soil moisture decrease along each transect from wetland center to upland).

We quantified hydrologic variation using a combination of water level, elevation surveys, and a 1m digital elevation model (S. Lee et al., 2019)). We estimated inundation extent at each wetland using daily water level and the digital elevation model (Jones et al., 2018a), and estimated water level at soil chamber points by interpolating between the inundation boundary and water level at the upland end of each transect (Figure 1.2a; (Maietta et al., 2020). Using each of these daily water level time series, we derived time series of the magnitude and direction of water level change over the previous 1-7 days ($WL_{1\text{-}7}$ and $\Delta WL_{1\text{-}7}$). We then summarized hydrologic variability over the water year at each chamber location by calculating the average and range in water levels, and the frequency and maximum duration of periods with negative or positive water levels. We summarized hydrologic variability at the wetland scale using surface water extent time series to calculate the cumulative proportion of area inundated throughout the year ("inundation index").

### Methane flux measurements

Methane emissions were calculated using monthly measurements at each wetland across the 2018 water year. Different techniques were used to quantify diffusive fluxes from inundated and non-inundated zones of each wetland. For inundated areas we used the turbulent boundary layer method with 3 replicate measurements of dissolved gas concentrations sampled near wetland centers and a gas exchange model for wind-sheltered water bodies (Cole et al., 2010; Poindexter & Variano, 2013). Atmospheric concentrations of methane were also sampled at each wetland for every

set of replicate headspace samples. Dissolved gas and equilibrium concentrations were calculated from partial pressure using Henry's Law constants, atmospheric concentrations, air pressure, and water temperature following (Cawley, 2018):

$$Flux_{inundated} = k \times \left(C_w - C_{eq}\right) \quad \text{(Equation 1.1)}$$

We were not able to include any gas fluxes associated with ice-out processes or effects of surface films that can impede gas transfer across air-water interfaces especially in forested swamps (Happell et al., 1995).

Fluxes from non-inundated areas were calculated from 24 hour incubations of 1-2 L static flux chambers installed along wetland transects (Figure 1.2) (Davidson et al., 2002). We only collected measurements from chambers with < 2 cm of standing water, resulting in a different number of measurements for each sampling period (i.e. we did not do incubations of submerged chambers). Chambers were constructed from the top portion of 5 L buckets affixed with air-tight screw top Gamma Seal © lids that enclosed between 1 and 2 L of air when sealed. Chamber collars were installed at least 2 weeks prior to the initial sampling period. Chamber lids were modified to include both a vent to equilibrate pressure changes in the environment (Davidson et al., 2002) as well as a sampling port with a valve from which 30 mL gas samples were collected at the beginning and end of each incubation. Although monthly sampling may not adequately capture the full range of variability in emissions, our intention was to assess the extent to which the seasonal hydrology might explain observed variability in fluxes. This design allowed for sampling all study wetlands over a 2-day period. All gas samples were analyzed on an SR 8601 gas

chromatograph equipped with a flame ionization detector and a Poropak column with a 3-point calibration curve. Flux rates were calculated from the difference in headspace partial pressure at the beginning and end of the incubation period, chamber-specific interior dimensions, average air temperature and pressure from the incubation period, and the gas constant R (Pedersen et al., 2010).

$$Flux_{non-inundated} = \frac{\frac{\Delta ppm}{time} \times \frac{vol}{area}}{\frac{1}{P} \times R \times T} \qquad \text{(Equation 1.2)}$$

Interior chamber volume was calculated for each sampling period as a cylinder based on the bucket diameter and an average of 4 measurements of the height of the chamber between the soil surface and lid position (~2-4 inches). Chamber fluxes less than an absolute value of 0.001 ppm were considered below the minimum detectable change and were set to 0 for subsequent analysis. Along with each chamber incubation, we measured volumetric water content and temperature at 3 points surrounding each chamber using a FieldScout TDR 150 soil moisture meter (Spectrum Technologies) with 3.8 cm rods. Soil moisture was calculated as water-filled pore space using volumetric water content and bulk density, which was measured once at each measurement point during the study.

The relationship between hydrologic metrics (Table 1.2) and methane fluxes was evaluated using generalized linear mixed effects models using wetland site as a random effect. Stepwise regression was used to evaluate fixed effects, including air and soil temperature, and remove highly correlated effects and model fit was evaluated using Akaike information criterion and marginal $R^2$ values. The magnitude

of flux rates from inundated, and non-inundated source and sink areas were compared using Wilcoxon signed rank tests.

### Spatial extent of methane emissions

To analyze the lateral boundary between net methane sources and sinks, we assessed whether the source area expanded and contracted over time in accordance with hydrologic conditions, or alternatively, if the transition was a relatively fixed location at each wetland. To do this, we used logistic mixed effect models to evaluate whether metrics representing point-scale hydrology (described above) or location were stronger predictors of whether a measured flux was positive or negative.

### Wetland-scale flux models

To compare approaches for upscaling to the wetland scale, we calculated emissions for each wetland using four simple models with different assumptions regarding methane source areas (Figure 1.3, Table 1.3). Wetlands were modeled as three concentric zones with differing flux rates: a central inundated "source" zone with positive emissions, a surrounding non-inundated source zone, and an outer non-inundated "sink" zone with methane uptake. The models vary based on which zones are included in calculating emissions, and whether the size of the inundated zone varied. Model I assumed emissions are from a fixed inundated area throughout the year (hereafter, *fixed-area* model). Model II calculated fluxes from inundated area time series, with no emissions from non-inundated zones (*variable-area, excluding non-inundated*). Model III included emissions from both inundated and non-inundated source areas (*variable-area, including all sources*), and Model IV

calculated net emissions from all three zones (*variable-area, sources and sinks*). Each model was run 1,000 times for each wetland at the daily time scale for one year, with inputs derived from the field measurements described above. Wetland-specific water level time series were fixed, but daily inputs of both non-inundated source zone buffer widths and flux rates for each of the three emission zones were sampled from distributions fit to the relevant observations averaged for each site.

*Results*

**Methane flux rates and water level**

Overall, flux rates showed high variability and differed significantly between wetland zones (Figure 1.4; $p < 0.001$). Inundated zone fluxes averaged $1.36 \pm 2.08$ mmol $m^{-2}$ $d^{-1}$ and non-inundated zone fluxes averaged $0.07 \pm 0.4$ mmol $m^{-2}$ $d^{-1}$. No positive emissions were measured from points with water level -90 cm below the soil surface; however, uptake was measured across a wide range of water levels, including from fully saturated soils. On average, water levels varied a range of 130 cm throughout the year with minimums in late October 2017 and late September 2018 and maximums during March 2018 (Figure 1.2; Table 1.1).

Mixed effect models indicated that flux rates from inundated soils were best explained by the direction of water level change ($\Delta WL_1$; $R^2 = 0.39$) and were not significantly related to water level. These fluxes were ~55% lower when water levels had risen rather than fallen since the previous day (Table 1.4; Figure 1.5). Water levels were also not a significant predictor of fluxes from non-inundated soils:

variability was best explained by soil moisture and the direction of water level change over the previous week ($\Delta WL_7$; $R^2 = 0.26$). Fluxes from non-inundated soils were approximately 32% lower when the water level had risen rather than fallen over the previous week (i.e., methane fluxes were greater when water level was receding). However, the model for non-inundated soils had low explanatory power and was unable to adequately capture the variance in our observations. Residuals showed consistent underprediction of the largest 10% of measured fluxes (> 0.1 mmol $m^{-2}$ $day^{-1}$). Dissolved methane concentrations were highly variable and ranged over two orders of magnitude (0.54–71 μmol $L^{-1}$). This variability was not correlated with water level or temperature, however we observed peaks at all sites in late summer, coincident with the lowest water levels and highest temperatures (Figure 1.6).

Average flux rates over the course the year were significantly correlated with metrics summarizing hydrologic variability at each measurement point (Figure 1.7). Median water level ($\rho = 0.83$, $\rho = 0.83$, $p < 0.05$) and duration of inundation ($\rho = 0.82$, $\rho = 0.83$, $p < 0.05$) had strong positive correlations with average log fluxes. Metrics describing hydrologic variability were largely correlated with each other, except for the frequency of dry periods (i.e., when water level < 0), which was not correlated with flux rates. Range and standard deviation of water level had weak negative correlations with range and standard deviation of flux rates ($\rho \sim -0.40$, $p < 0.05$).

**Spatial extent of source and sink zones**

We observed both methane emissions and uptake over wide and overlapping ranges of hydrologic conditions. Nearly all measurement points transitioned between being methane sources during generally wetter conditions and methane sinks during drier conditions. However, we measured positive fluxes from locations with water levels as low as ~80 cm below the soil surface and up to ~8 m outside of the wetland boundary, and occasionally measured negative fluxes from points with fully saturated (but not inundated) soils.

The distinction between source and sink measurements was better explained by variables associated with hydrologic conditions rather to those associated with measurement position. Water level, direction of water level change, and soil moisture together explained 55% of the difference between source and sink measurements, whereas the position of measurement locations only explained 20% (Table 1.5). According to the best fitting model, positive emissions were more likely when water levels had fallen since the previous day, when the water level was above -25 cm, or when soil moisture exceeded ~70% water filled pore space (Figure 1.8).

**Wetland-scale flux rates**

Wetland-scale emissions estimates were the highest using the fixed area model (i.e., assuming no changes in inundation extent), and lowest using the variable-area model that excluded non-inundated regions (Figure 1.9, 1.10). Estimates calculated using all sources and sinks were not significantly lower than those using the variable area all sources model. In Model IV, on average 94% of emissions were from the inundated zone. Emissions estimated using variable inundation extents were between 57–74%

of the emissions calculated under the fixed-area model. This difference was positively correlated with the inundation index ($\rho = 0.73$, $p < 0.001$) and negatively correlated with methane flux rates ($\rho = -0.69$, $p < 0.001$), meaning the largest discrepancies from the fixed area model were for wetlands with a low inundation and high methane flux rate. Uncertainty was highest for wetlands with the largest variability in inundation zone methane flux rates.

*Discussion*

Overall, we found that hydrologic variability—particularly the inundation extent and duration—was an important predictor of wetland-scale methane flux rates from forested mineral soil wetlands. Inundated soils were consistently a source of methane; and much of the variability in these fluxes was explained by direction of water level change, and surprisingly, not water level itself. Intermittently inundated soils alternated between being methane sources and sinks depending on hydrologic conditions. Below we discuss how the wetland hydrologic regime may be controlling methane production and emissions from mineral soil wetlands, and how this variability affects upscaling of freshwater methane emissions from wetland to regional scales.

**Effects of hydrologic variability on methane fluxes**

Inundated soils were the dominant source of methane emissions. Standing water had high, but variable concentrations of dissolved methane that were similar in magnitude to concentrations found in other small open water ecosystems (Table 1.6). The

observed concentrations exceed values typical of both larger lakes (< 2 μmol $L^{-1}$; (Bastviken et al., 2004; Holgerson & Raymond, 2016a)) and flowing waters (1.35 ± 5.16 μmol $L^{-1}$; (Stanley et al., 2016)). Variability was not explained by water level above the soil surface, which suggests that once wetlands are inundated, subsequent changes in water level do not have a strong effect on rates of production and consumption of methane within standing water. Effects of water depth on methane concentrations and fluxes may only occur over a larger range of water levels than we observed (> 1.5 m) or over shorter time periods than monthly sampling could capture. This pattern is broadly consistent with findings of a recent global synthesis, showing seasonally averaged emissions sharply increase up to a critical water level above the soil surface, above which there is high variability (Calabrese et al., 2021).

Because the direction of water level change was a better predictor of flux rates than water level, this may indicate a lagged relationship between water level and methane emissions as has been found for other freshwater wetlands where water table depth is a major predictor (Knox et al., 2021). When soils are unsaturated, alternate electron acceptors such as ferric iron and sulfate may re-oxidize and provide substrate for microbes that use more thermodynamically favorable pathways to then outcompete methanogens (Estop-Aragonés et al., 2012; Jeffrey et al., 2019; Ratering & Conrad, 1998). Such an effect would suppress methane production after periods of lower water levels and explain why we observed lower methane fluxes during rising rather than falling water levels. Increasing water levels can also reduce the supply of organic substrate for methanogens through dilution and effects to productivity of aquatic

vegetation (Calabrese et al., 2021). Additionally, changes in water level relative to the groundwater table could affect lateral transport of dissolved methane into wetland surface water through shallow subsurface flowpaths controlled by hydraulic gradients, especially for mineral soil wetlands with higher labile carbon pools. This lateral transport can concentrate methane produced in deeper soil layers of the surrounding wetland catchment, resulting in spatial discontinuities between factors driving methane production (e.g. water level, soil carbon content), oxidation, and emission. Lateral flowpaths are common in wetland-rich landscapes like the Prairie Pothole Region and the Delmarva Peninsula (Hayashi et al., 2016; Phillips & Shedlock, 1993a).

Average methane fluxes at each measurement point were correlated with metrics summarizing the duration but not frequency of inundation. This aligns with other studies that found large fluxes associated with flooding induced inundation (Chamberlain et al., 2016; Gatland et al., 2014) and continuous saturation (Altor & Mitsch, 2008). The frequency of wetting and drying cycles may be related to methane flux potential in soils (Kannenberg et al., 2015), but have complex interactions with vegetation and the timing of drying/drainage such as in efforts to mitigate emissions from flooded rice agriculture (Yan et al., 2005).

The relationship between wetland hydrology regime and methane emissions has implications for total freshwater wetland emissions in the US because recent trends show losses of coastal forested wetlands and gains in wetland types with more stable

water levels such as farm ponds and created wetlands on previously drained mineral soil (Dahl, 2011b; M. Lang et al., 2020). Our results suggest that this trend could be leading to higher net methane emissions because of increased inundation, however there are also plausible mechanisms for increased frequency of wet-dry cycles in forested wetlands to result in higher emissions.

### Spatial extent of methane uptake and emissions

Fluxes from non-inundated soils transitioned between uptake and emissions depending on hydrologic conditions, and flux rates were only partially explained by soil moisture and the direction of changes in water level. Our findings align with the emerging conceptual framework for peatland soils that a distinct vertical separation between zones of methane production and consumption is unlikely, and that fluxes are mainly controlled by other environmental factors that are linked to hydrologic dynamics in complex ways (Yang et al., 2017). This is especially relevant in low-gradient landscapes with shallow groundwater tables where large areas of mineral soil can become inundated (or pass a soil moisture threshold for methane emissions) with even small changes in water levels (Spahni et al., 2011). Under these circumstances, methane source areas will not be limited strictly to wetland soils. Our results suggest appropriately representing methane source areas in emission models requires improved modeling of hydrologic processes that lead to inundation of small-scale features like topographic depressions and ditches (Peacock et al., 2021).

Methane uptake was not limited to unsaturated soils, but rather occurred under a wide range of hydrologic conditions potentially by different microbial communities. Maietta et al. (2020) analyzed the microbial community composition from soils collected at the same measurement points used in this study and found methane oxidizers along a wider range of the hydrologic gradient compared to methanogenic archaea. Flux measurements align with results of the microbial community composition, showing there is a capacity for both methanogenesis and methane consumption within and slightly upland of intermittently inundated soils. Although additional factors such as low soil pH may limit net emissions from these systems, (Le Mer & Roger, 2001) these results underscore the need for considering both methane consumption and production in wetland emission models in order to accurately predict net fluxes.

### Inundation extent as a proxy for methane source areas

The methane emissions source area of our study sites could reasonably be approximated by a time series of surface water extent because the actual source area included minimal emissions from surrounding non-inundated soils. Areal wetland-scale flux rates were substantially lower (26–43%) in models that accounted for inundation variability. One way to incorporate this seasonal drying is to use a correction factor when scaling up methane flux rates from similar small water bodies in landscape or regional assessments that do not otherwise quantify hydrologic variability. Similarly, experimental work in Prairie Pothole wetlands (Tangen & Bansal, 2019) and on small water bodies in Australia (Grinham et al., 2018a) calls for

incorporating hydrologic variability when scaling up flux rates. Our models showed that a reasonable approximation of diffusive emissions would be scaling wetland area by 64%, which surprisingly matches the variability in surface area for the smallest size class water bodies reported by Grinham et al (2018a). We account for minimal fluxes from non-inundated zones but inundated zones contributed the overwhelming majority of emissions in our models (83–99%). Across a long-term dataset of emissions from Prairie Pothole wetlands, Tangen and Bansal (Tangen & Bansal, 2019) also found that continuously wet zones accounted for >85% of cumulative fluxes. Using this correction factor approach relies on a reference wetland boundary, which for Grinham et al (2018a) was based on analyzing a time series of high-resolution aerial imagery. We determined these areas empirically during our study period, however reliable maps of small water bodies, especially forested wetlands, are rare.

Our study suggests that seasonally inundated forested wetlands are substantial sources of methane at the landscape scale in the Upper Choptank River watershed. Emission estimates from the variable area sources and sink model (IV) indicate an average areal flux rate of at least 1.65 kg $m^{-2}$ $yr^{-1}$, which is four orders of magnitude greater than the average methane uptake rate in temperate forest soils 11/11/21 12:24:00 PM, even after accounting for a small amount of uptake within the wetland. Across the Upper Choptank River watershed, a third of the land is forest and forested wetlands. Hydrologic classifications in the National Wetlands Inventory suggest that almost 30% of that area is non-riverine freshwater wetlands subject to at least temporary or

intermittent flooding (Table 1.7) and therefore potential sources of methane emissions. Improved methods for detecting and modeling surface water dynamics in low relief landscapes will greatly improve our ability to quantify methane emissions from forested wetlands.

*Conclusions*

Understanding controls on methane fluxes in wetlands is needed to account for them properly in earth system models and to predict impacts of changing land cover and climate. We demonstrate that quantifying the hydrologic regime of seasonally inundated forested freshwater wetlands enables a more accurate estimation of their methane emissions. Hydrologic variability helped explain whether methane fluxes were positive or negative, and flux rates were lower during rising rather than falling water levels. Future work should assess the role of methane oxidation in reducing net evasion of methane from wetlands with standing water. We found that intermittently flooded soils transitioned between methane sources and sinks depending on hydrologic conditions; and using spatially explicit models, we found that the majority of methane emissions could be estimated from the inundated portions of these wetlands.

**Table 1.1**. Properties of wetland study sites. Values are mean ± standard deviation and (range).

| | Max area inundated ($m^2$) | Inundation index | Water level (m) | NRCS soil type | Soil bulk density ($g\ m^3$) | Dissolved $CH_4$ ($\mu mol\ L^{-1}$) | DOC ($mg\ L^{-1}$) | Inundated flux rate ($mmol\ m^{-2}\ day^{-1}$) | Non-inundation source flux rate ($mmol\ m^{-2}\ day^{-1}$) | Non-inundated sink flux rate ($mmol\ m^{-2}\ day^{-1}$) | Buffer distance (m) | Scale Factor |
|---|---|---|---|---|---|---|---|---|---|---|---|---|
| W1 | 1,920 | 0.56 | 0.39 (0 - 0.71) | Hammonton-Fallsington-Corsica | 0.070 | 22.0 ± 23 (n = 32) (1.1 – 58.3) | 34.8 | 2.97 ± 3.1 (n =10) | 0.40 ± 0.90 (n = 16) | -0.003 ± 0.002 (n = 28) | 5.4 ± 4.7 | 0.62 |
| W2 | 597 | 0.58 | 0.63 (0.17 - 1.09) | Hammonton-Fallsington-Corsica | 0.448 | 7.6 ± 9 (n = 33) (0.5 – 24.0) | 34.6 | 1.02 ± 1.2 (n = 9) | 0.16 ± 0.48 (n = 10) | -0.004 ± 0.004 (n = 29) | 1.7 ± 2.7 | 0.61 |
| W3 | 2,065 | 0.56 | 0.61 (0.22 - 0.93) | Corsica mucky loam | 0.239 | 16.8 ± 21 (n = 29) (5.7 – 71.1) | 40.9 | 2.27 ± 2.9 (n = 9) | 0.08 ± 0.16 (n = 15) | -0.004 ± 0.003 (n = 27) | 2.9 ± 2.7 | 0.57 |
| W4 | 1,639 | 0.72 | 0.60 (0.17 - 1.03) | Hammonton-Fallsington-Corsica | 0.267 | 2.8 ± 2.6 (n = 29) (0.8 – 9.5) | 24.8 | 0.38 ± 0.35 (n =10) | 0.07 ± 0.12 (n = 9) | -0.003 ± 0.001 (n = 37) | 1.8 ± 1.8 | 0.74 |
| W5 | 1,710 | 0.57 | 0.40 (0.04 - 0.70) | Lenni loam | 0.267 | 3.1 ± 1.9 (n = 23) (1.2 – 6.9) | 29.7 | 0.41 ± 0.26 (n = 8) | 0.18 ± 0.60 (n = 19) | -0.003 ± 0.001 (n = 29) | 6.3 ± 4.2 | 0.69 |
| W6 | 380 | 0.60 | 0.34 (0.15 - 0.46) | Hammonton-Fallsington-Corsica | 0.184 | 14.7 ± 9.8 (n =25) (3.6 – 35.8) | 27.0 | 1.98 ± 1.3 (n = 8) | 0.37 ± 0.92 (n = 13) | -0.003 ± 0.003 (n = 13) | 2.2 ± 2 | 0.63 |

**Table 1.2**. Areas represented in each of the four inundation models. See section 2.4 for details. Wetland boundary is defined from the maximum observed inundation extent during the period of study.

| Category | Description |
|---|---|
| ***Daily values (point scale)*** | Water level |
| | Magnitude of water level change over previous 1-7 days |
| | Direction of water level change over previous 1-7 days |
| | Precipitation |
| | Total precipitation over previous 1-4 days |
| | Soil moisture |
| | Soil temperature |
| ***Annual values (point scale)*** | Average and range of water level |
| | Water level standard deviation and coefficient of variation |
| | Number of times water level < 0 |
| | Number of times water level < 0 for more than 1 day |
| | Maximum duration of water level < 0 |
| | Number of times water level > 0 |
| | Number of times water level > 0 for more than 1 day |
| | Maximum duration of water level > 0 |
| ***Annual values (wetland scale)*** | Inundation index |

**Table 1.3**. Regression parameters for random intercept mixed effect models explaining variability of methane flux rates measured from inundated and non-inundated soils. Wetland site is included as a random effect. $\Delta WL_1$ and $\Delta WL_7$ are the direction of water level change (increasing or decreasing) over the previous one and seven days respectively.

| | **Inundated source zone** | **Non-inundated source zone** | **Non-inundated sink zone** |
|---|---|---|---|
| *Model I* | Wetland boundary | Not included | Not included |
| *Model II* | Daily surface water extent | Not included | Not included |
| *Model III* | Daily surface water extent | Daily estimate of buffer surrounding surface water extent | Not included |
| *Model IV* | Daily surface water extent | Daily estimate of buffer surrounding surface water extent | Remainder between wetland boundary and source zones |

**Table 1.4**. Regression parameters for random intercept mixed effect models explaining variability of methane flux rates measured from inundated and non-inundated soils. Wetland site is included as a random effect. $\Delta WL_1$ and $\Delta WL_7$ are the direction of water level change (increasing or decreasing) over the previous one and seven days respectively.

**Inundated zone**

| | | | |
|---|---|---|---|
| Conditional $R^2$ | 0.39 | | |
| Marginal $R^2$ | 0.12 | | |
| | *Estimate* | *t* | *P-value* |
| Intercept | 0.08 | 0.287 | 0.78 |
| $\Delta WL_1$ | -0.81 | -3.149 | <0.005 |

**Non-Inundated zone**

| | | | |
|---|---|---|---|
| Conditional $R^2$ | 0.26 | | |
| Marginal $R^2$ | 0.19 | | |
| | *Estimate* | *t* | *P-value* |
| Intercept | -3.40 | -28.80 | <0.005 |
| $\Delta WL_7$ | -0.30 | -3.77 | <0.005 |
| Water filled pore space | 0.02 | 6.01 | <0.005 |

**Table 1.5**. Regression model parameters for probability of positive emissions as a function of predictors associated with hydrologic variability and measurement position.

**Hydrologic variability**

| | | | |
|---|---|---|---|
| Conditional $R^2$ | 0.58 | | |
| Marginal $R^2$ | 0.55 | | |
| | *Estimate* | *z* | *P-value* |
| Intercept | -0.83 | -0.63 | 0.53 |
| Water level | 0.04 | 3.39 | <0.001 |
| $\Delta WL_1$ | -1.43 | -3.66 | <0.001 |
| Water filled pore space | 0.04 | 2.15 | 0.03 |

**Measurement position**

| | | | |
|---|---|---|---|
| Conditional $R^2$ | 0.21 | | |
| Marginal $R^2$ | 0.20 | | |
| | *Estimate* | *z* | *P-value* |
| Intercept | 1.31 | 2.61 | <0.01 |
| Relative elevation | -2.33 | -3.51 | <0.001 |
| Distance from wetland boundary | -0.03 | -0.59 | 0.55 |

**Table 1.6.** Methane data from small open water ecosystems. N is the number of individual systems Values are average ± std dev and/or range (low–high).

| System type | $CH_4$ Concentrations (μmol $L^{-1}$) | $CH_4$ Fluxes (mmol $m^{-2}$ $day^{-1}$) | N | Reference |
|---|---|---|---|---|
| **Forested wetlands/ponds** | 27 ± 4.6 (0.4 – 210) | 10.8 ±18.5 (0.2 – 73) | 4 | Kifner et al 2018 |
| | 11.3 ± 15.6 (0.54 – 71) | 0.38 – 2.97 | 6 | *This study* |
| | 33.4 (21.0 – 58.9) | 10.6 ± 0.13 | 6 | Holgerson 2015 |
| | | (-0.12 to 3.36) | 3 | Morse et al 2012 |
| **Prairie pothole wetlands** | 0.2 – 34.3 | 5.1 (0.30 – 36.5) | 2 | Martins et al 2017 |
| | 6.1 – 15.7 | 0.7 – 13.3 | 3 | Bortolotti et al 2016 |
| | | (0.1 – 3.8) | 62 | Baidou et al 2011 |
| | | 0.63 ± 0.05 (-0.06 – 4.36) | 1 | Bansal et al 2018 |
| | | (0.06 – 243.10) | 119 | Tangen et al 2015 |
| | | (0.46 - 22.32) | 88 | Tangen and Bansal 2019 |
| **Agriculture/aquaculture ponds** | 2.29 – 50.48 | 4.56 (2.16 – 55.68) | 3 | Yang et al 2019 |
| | | 7.2 ± 1.74 | 77 | Ollivier et al 2019 |
| | | 0.93 – 87.58 (0.06 – 338.15) | 22 | Grinham et al 2019 |
| | | 16.43 ± 1.06 | 3 | Yuan et al 2019 |
| **Urban/stormwater ponds** | 1.62 (0.11 – 20.23) | 1.89 (0.02 – 10.85) | 40 | Peacock et al 2019 |
| | | 0.93 – 36.78 | 7 | Herrero Ortega et al 2019 |
| | | 1.25 ± 18.70 | 1 | van Bergen et al 2019 |
| | | 22.59 (0.45 – 114.14) | 15 | Gorskey et al 2019 |
| **Boreal/permafrost thaw ponds** | 9 (0.02 – 47) | | 146 | Polishchuk et al 2018 |
| | 3 – 40 | (6.86 – 11.2) | 30 | Hamilton et al 1994 |
| | 0.3 – 6.2 | (0.01 – 12.8) | 7 | Matveev et al 2016 |
| | 0.04 – 5.17 | (0.03 – 5.62) | 52 | Laurion et al 2010 |
| | 24 ± 3 | 9.35 ± 0.27 | 52 | Kuhn et al 2018 |
| | 1.1 | (1.3 – 2.3) | 1 | Dabrowski et al 2020 |
| | | (0.22 – 0.47) | 2 | Huttunen et al 2002 |
| **Beaver ponds** | (7.1 – 17.3) | 9.35 | 2 | Yavitt et al 1992 |
| | | 15.6 (0.06 – 87.3) | 1 | Yavitt et al 1990 |
| | | (8.66 – 57.3) | 4 | Bubier et al 1993 |
| | | (0.87 – 1.0) | 2 | Ford and Naiman 1988 |
| | | 2.3 ± 1.9 | 1 | Weyhenmeyer 1999 |
| | | 5.87 | 1 | Roulet et al 1997 |
| | | 5.8 - 5.3 (1.12 – 34.66) | 3 | Lazar et al 2014 |

**Table 1.7.** Area and percentage of land cover classes overlapping palustrine wetlands in Upper Choptank River watersheds Tuckahoe Creek (HUC 0206000501) and Watts Creek (HUC 0206000502). Area subject to at least seasonal flooding intersects wetland polygons with NWI water regime modifiers C, E, F, and H (Seasonally Flooded, Seasonally Flooded/Saturated, Semi-permanently Flooded, and Permanently Flooded); area subject to temporary or intermittent flooding intersects wetland polygons with all seasonal flooding categories and those with modifiers A and J (Temporarily Flooded and Intermittently Flooded). Forest land cover is NLCD classes 41, 42, and 43 (Deciduous Forest, Evergreen Forest, Mixed Forest); Woody wetlands are class 90 and cultivated crops are class 82.

| | | **Tuckahoe** | **Watts Creek** | **Combined** |
|---|---|---|---|---|
| | Watershed area | 399.7 $km^2$ | 670.7 $km^2$ | 1,069.6 $km^2$ |
| ***Land cover*** | Freshwater wetlands (NWI) | 12.8%<br>51.19 $km^2$ | 17.4%<br>116.79 $km^2$ | 15.7%<br>167.98 $km^2$ |
| | Woody Wetlands (NLCD) | 16.3%<br>65.3 $km^2$ | 23.7%<br>158.3 $km^2$ | 20.9%<br>223.5 $km^2$ |
| | Forest (NLCD) | 11.2%<br>44.7 $km^2$ | 13.2%<br>88.4 $km^2$ | 12.4%<br>133.1 $km^2$ |
| | Cultivated crops (NLCD) | 65.2%<br>260.4 $km^2$ | 54.3%<br>364.1 $km^2$ | 58.4%<br>624.5 $km^2$ |
| ***Areas subject to at least seasonal flooding*** | Forest & woody wetlands | 19.9%<br>21.9 $km^2$ | 18.1%<br>44.5 $km^2$ | 18.6%<br>66.4 $km^2$ |
| | Forest | 3.2%<br>1.4 $km^2$ | 2.1%<br>1.9 $km^2$ | 2.5%<br>3.3 $km^2$ |
| | Woody wetland | 31.3%<br>20.4 $km^2$ | 26.9%<br>42.7 $km^2$ | 28.3%<br>63.1 $km^2$ |
| ***Areas subject to at least temporary or intermittent flooding*** | Forest & woody wetlands | 39.1%<br>43.0 $km^2$ | 26.0%<br>64.0 $km^2$ | 30.0%<br>107.0 $km^2$ |
| | Forest | 8.7%<br>3.9 $km^2$ | 6.1%<br>5.4 $km^2$ | 6.9%<br>9.2 $km^2$ |
| | Woody wetland | 59.9%<br>39.1 $km^2$ | 37.1%<br>58.7 $km^2$ | 43.7%<br>97.8 $km^2$ |

**Figure 1.1**: Locations of six forested wetland study sites (W1-6) within the Upper Choptank River watershed (Tuckahoe Creek HUC 0206000501 and Watts Creek-Choptank River HUC 0206000502) and hydrologic regime classifications of National Wetland Inventory freshwater wetlands.

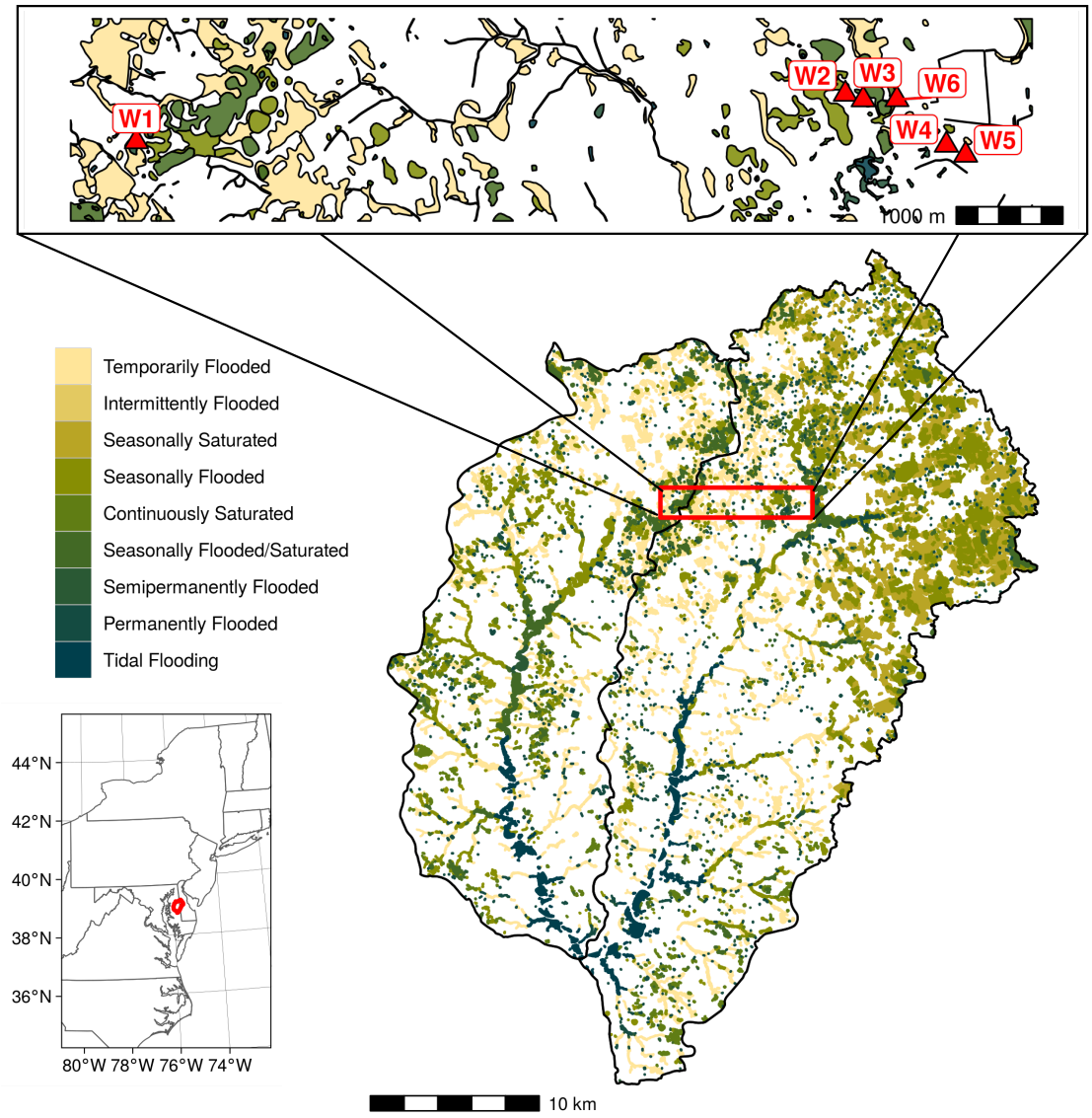

**Figure 1.2**: (a) Site design showing relative locations of wetland and upland surface water wells and soil flux chambers (not to scale); (b) Average (± sd) water level hydrographs at wetland well and chamber measurement points; (c) Topography, modeled inundation frequency, and locations of measurement points (dots) and wetland well (triangle) at one of the six wetland sites. Contour lines show 20 cm elevation increments from the lowest point of the wetland.

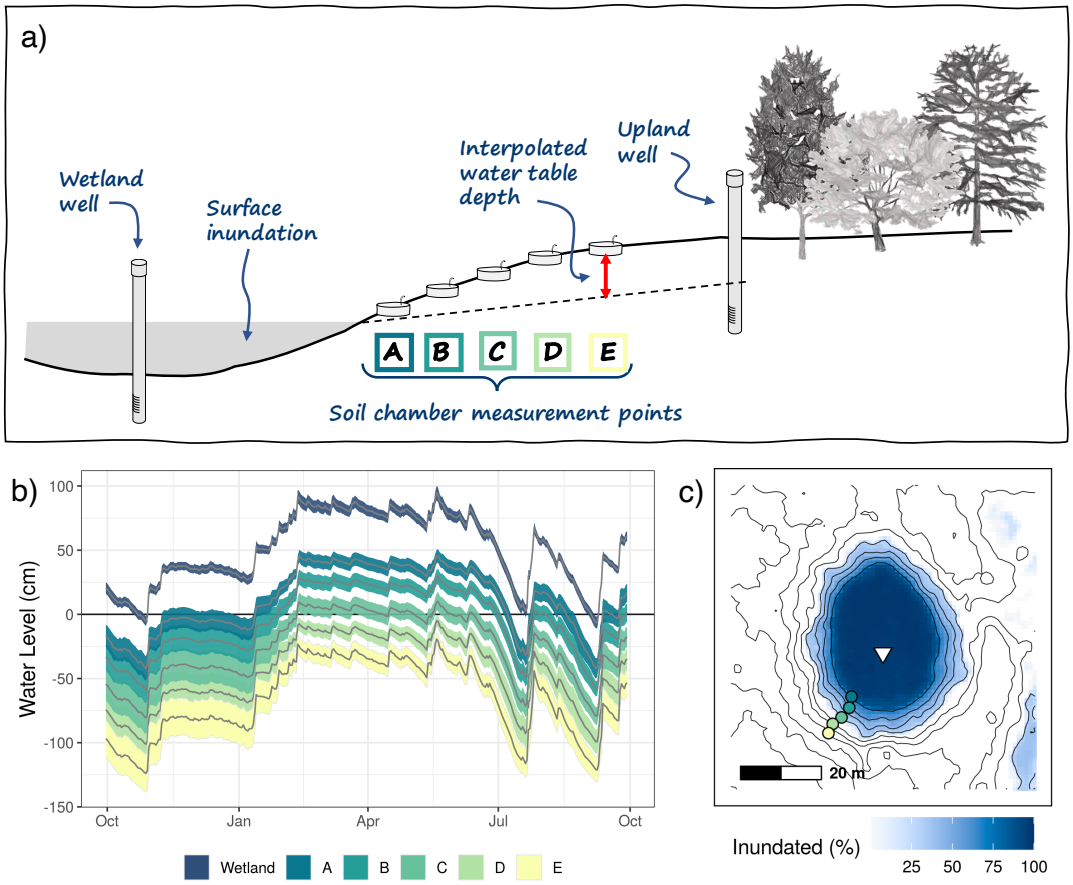

**Figure 1.3**: Overview of the four scaling models used to estimate wetland flux rates. Daily wetland-scale emissions are calculated from areal extent and flux rates from 1, 2, or 3 wetland zones. Inundated area used in variable area Models (II, III, and IV) is determined from mean daily water level. Non-inundated source area (Models III and IV) is calculated as a buffer around the inundated area with a width sampled from a distribution of wetland-specific observations. The area of the non-inundated sink zone (only in Model IV) was calculated as the difference between the wetland boundary and the combined area of the inundated and non-inundated source zones. Flux rates for each of the 3 zones were sampled from wetland-specific distributions of the relevant measurements.

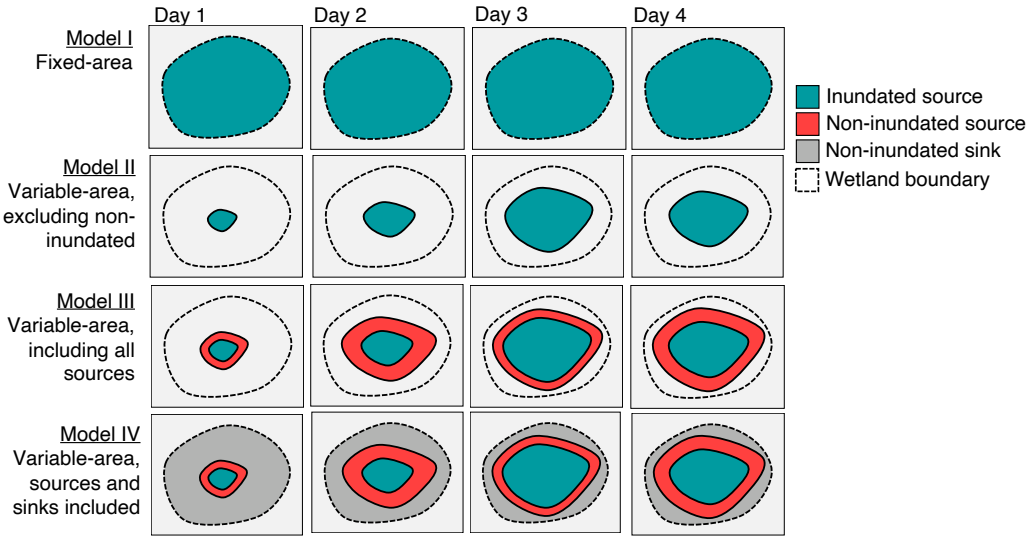

**Figure 1.4**: Relationship between water level and methane flux rates. In (a) only fluxes near 0 are shown for greater detail. Points above the horizontal line are positive emissions and points below the line are negative (uptake). In (b) all flux values are shown on a log scale. Points to the left of the vertical line are from non-inundated soils and points to right of the vertical line are measurements from inundated soils.

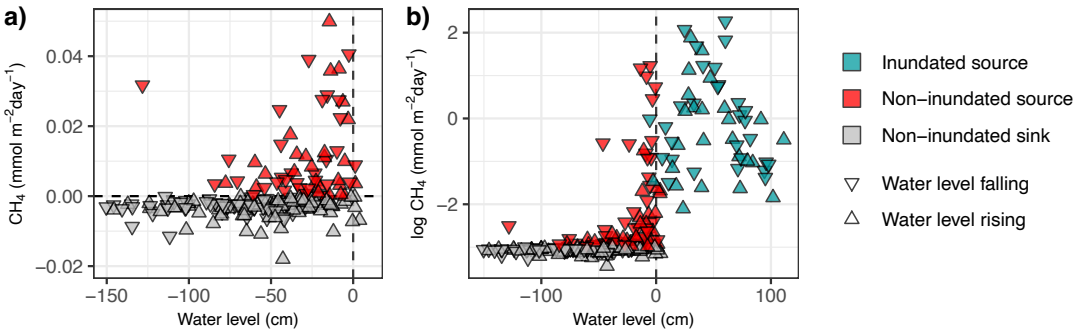

**Figure 1.5**: Comparison of measured flux rates in each wetland zone when water level had risen or fallen during previous 7 days.

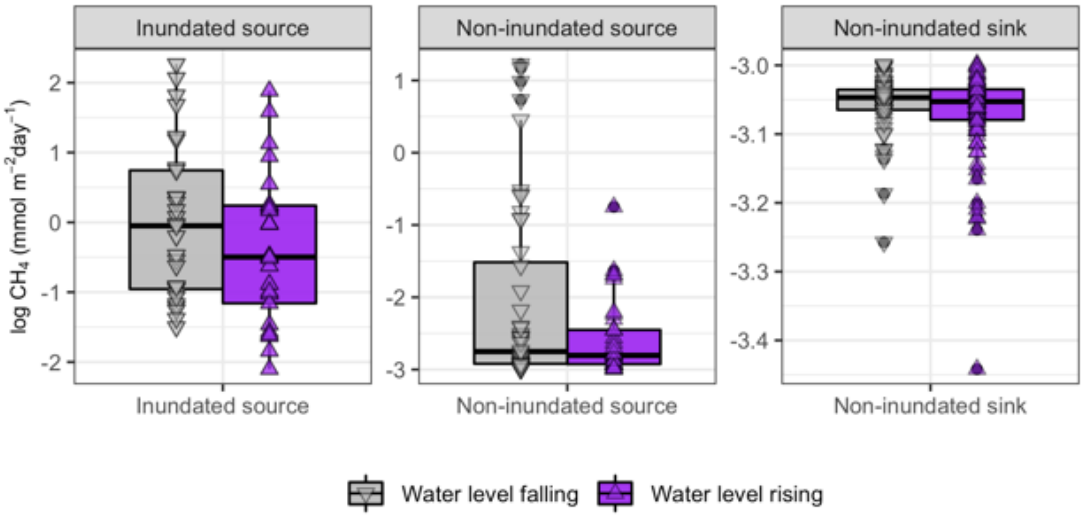

**Figure 1.6**: Seasonal patterns of air temperature and methane fluxes. a) daily air temperature from a nearby weather station, with orange points representing sampling events. Panels b, c, and d show monthly average flux rates by wetland site for inundated zones (b), non-inundated source zones (c), and non-inundated sink zones (d).

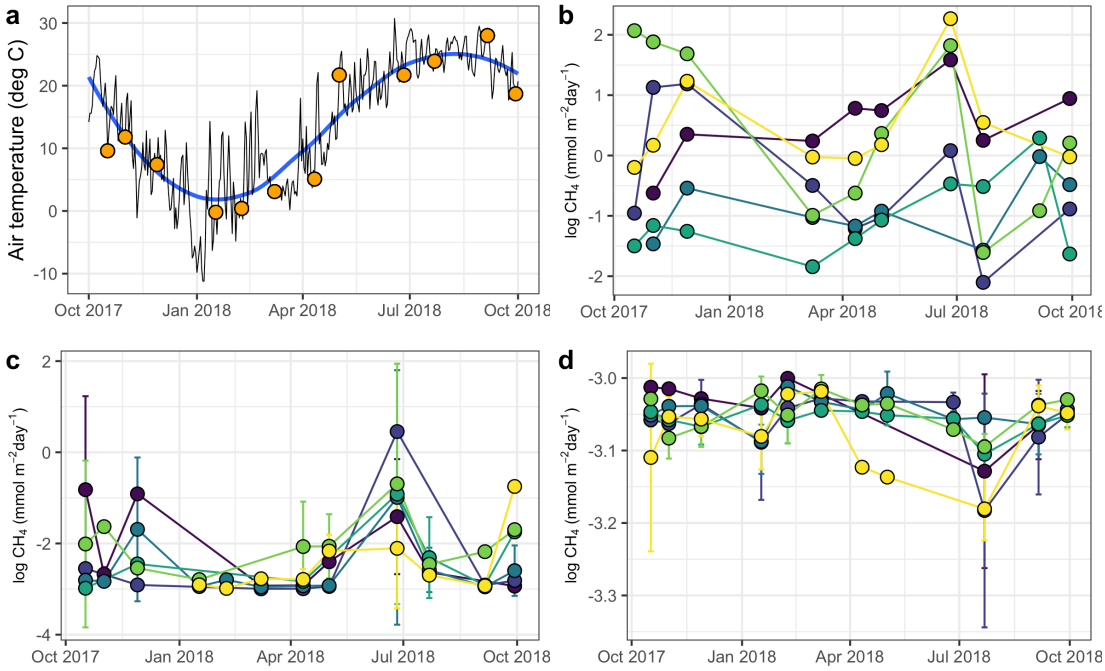

**Figure 1.7:** Correlation matrix between metrics summarizing hydrologic variability and methane flux rates at each measurement point. Nonsignificant correlations are indicated by X.

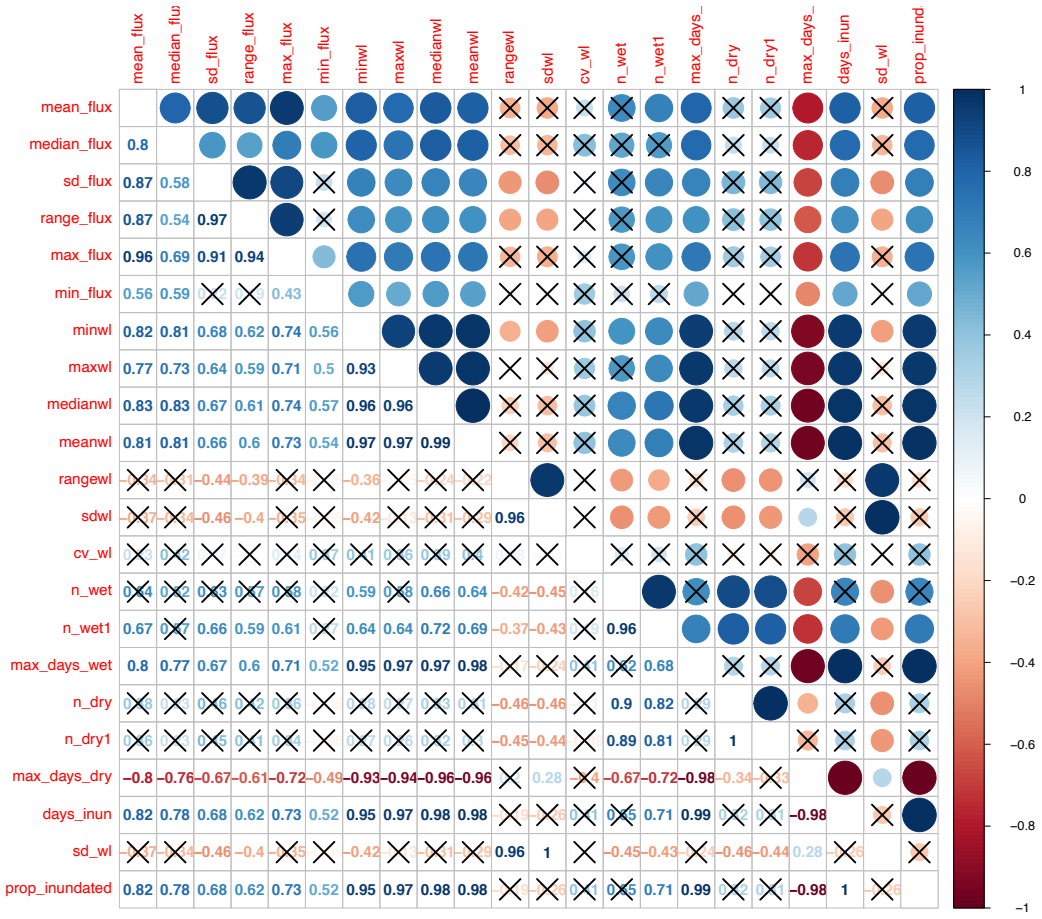

**Figure 1.8**: Distribution of hydrologic conditions (top) and measurement position (bottom) with positive (methane sources; red dots) and negative fluxes (methane uptake; gray dots). Lines show logistic models for the probability of positive emissions based on the value of each of the continuous variables.

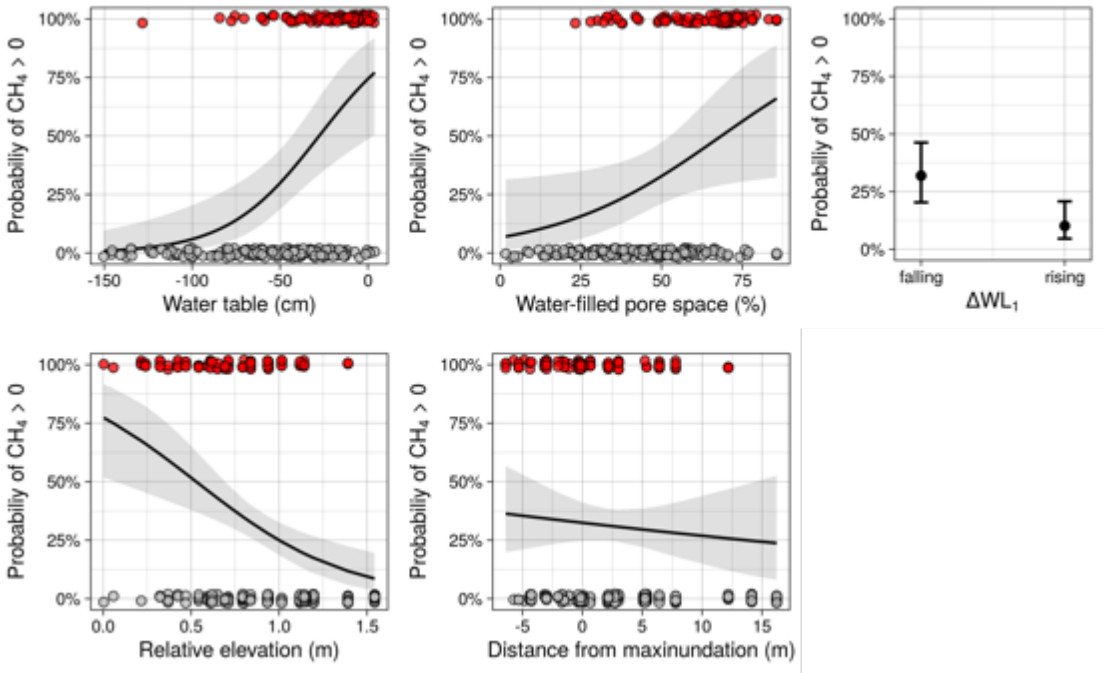

**Figure 1.9**: Average difference in annual upscaled wetland emissions calculated using different sets of assumptions regarding inundation dynamics (see text and Figure 1.33 for model details). Error bars represent standard deviation across the 6 study wetlands. Horizontal line at 64% indicates mean of Model IV.

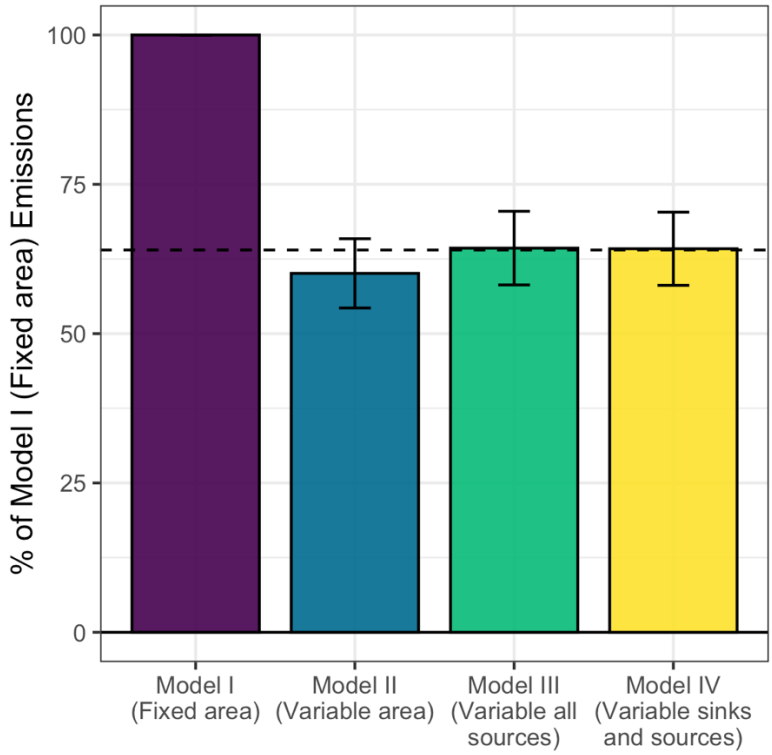

**Figure 1.10**: Average wetland-scale areal flux rates for each of the study wetlands calculated using different sets of assumptions regarding inundation dynamics (see text and Figure 1.3 for model details). Error bars represent 95% confidence intervals from 1,000 model iterations.

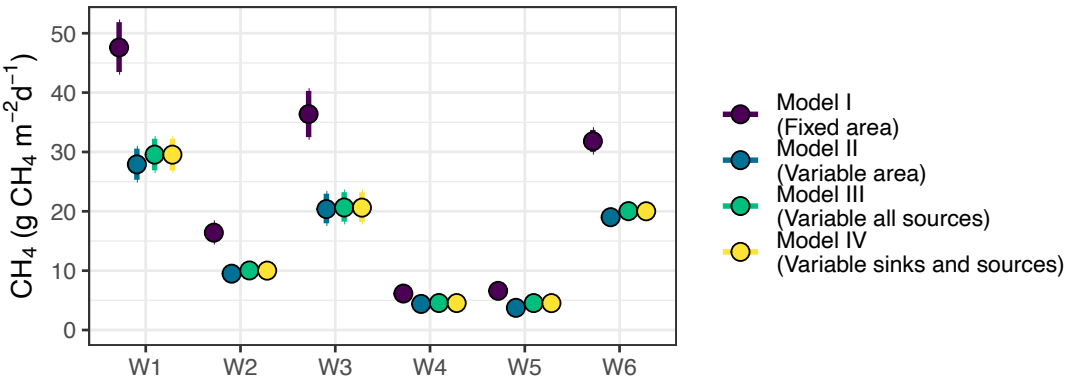

# Chapter 2: Effects of Using High Resolution Satellite-based Inundation Time Series to Estimate Methane Flues from Forested Wetlands

*Introduction*

Global change is affecting the quantity, quality, and timing of material fluxes through ecosystems with consequences for the fate and transformation of carbon. Inland waters are now recognized as fundamental to understanding the global carbon cycle (Cole et al., 2007; Raymond et al., 2013; Tranvik et al., 2009) yet our ability to characterize carbon fluxes and their drivers at landscape and regional scales remains limited by available data on surface water extent and dynamics—particularly for forested wetlands, very small water bodies (e.g. ponds), and areas with temporally varying inundation. Collectively, these limitations represent a major shortcoming in our ability to account for methane emission sources, and at least one third of all uncertainty in the global methane budget (Melton et al., 2013; Saunois et al., 2020b).

Methane emissions for lakes, ponds, reservoirs, streams, and rivers have been calculated by upscaling the best available data on flux rates and the areal extent of those waters by category (Saunois et al., 2020b). However, for wetlands, a combination of land cover maps, remote sensing data, and simulated hydrologic fluxes are used to calculate temporally varying methane producing areas as inputs to process-based biogeochemical models (Poulter et al., 2017b; Wania et al., 2012). Both approaches suffer from uncertainties associated with spatial and temporal

variation in inundation extent which is highly relevant for resolving sources and sinks of methane at global scales. This wetland extent problem contributes substantial uncertainty in methane budgets and limits our ability to identify drivers of recent increases in atmospheric concentrations (Thornton et al., 2016).

Upscaling empirical data on gas flux rates to quantify freshwater methane emissions is fraught with biases, including inadequate representation of underlying drivers (DelSontro et al., 2018a; Seekell et al., 2014) and lack of consideration of seasonal events such as ice-out or non-growing season emissions (Treat et al., 2018). Despite advances in remote sensing of aquatic systems, identifying small water bodies remains a challenge because they are often optically complex, obscured by vegetation, or below the resolvable size of satellite sensors (Allen & Pavelsky, 2018; Kuhn et al., 2019). The resulting omission of forested wetlands, small water bodies, and inundation dynamics in land cover and surface water data sets is broadly recognized (DeVries et al., 2017; M. W. Lang et al., 2020), but its implications for methane emissions accounting is unresolved (Poulter et al., 2017b; Thornton et al., 2016). This is despite recognition that headwaters and small water bodies play disproportionate roles in ecosystem processes (Hanson et al., 2007; Holgerson & Raymond, 2016b; Lowe & Likens, 2005) and may comprise the largest proportion of freshwater area (Bishop et al., 2008; Downing et al., 2006).

The ability to monitor and detect surface water at higher spatial and temporal resolution is advancing through new technologies including sub-pixel methods

(DeVries et al., 2017), fusion with hydrologic models (Evenson, Golden, et al., 2018), satellite constellations (Claverie et al., 2018; Cooley et al., 2019), and applications of machine learning (Jia et al., 2018; M. W. Lang et al., 2020; Lee et al., 2019). However, most remote sensing applications for freshwater bodies remain focused on relatively large or unvegetated systems (Griffin et al., 2018; Kuhn et al., 2019; Pekel et al., 2016b) by excluding pixels influenced by fractional coverage of soil and vegetation (Ji et al., 2009). Using such methods is warranted to avoid classification errors associated with spectral unmixing (Halabisky et al., 2016), but it can also result in large uncertainties for carbon fluxes at regional or global scales (Melton et al., 2013; Thornton et al., 2016; Treat et al., 2018) due to substantial underrepresentation of surface water extent (DeVries et al., 2017). Previous studies have explored inter-annual variability in wetland extent (Huang et al., 2014b; M. W. Lang et al., 2020; Yeo et al., 2019) but investigation of intra-annual dynamics has generally been limited by availability of cloud-free leaf-off imagery. Further, most investigations have not characterized inundation patterns for individual wetlands (M. K. Vanderhoof et al., 2018) or used sub-pixel estimation techniques (DeVries et al., 2017; Yeo et al., 2019) to account for the preponderance of small water bodies that result in mixed spectral signatures for pixels in 30 m resolution imagery.

Discrepancies between top-down and bottom-up emissions tend to be largest from forested areas (Melton et al., 2013). Recent investigations into these discrepancies have uncovered new sources and emission pathways from trees (Pangala et al., 2017). Further, in tropical regions, wetland emission models underestimate emissions

compared to observations with the largest discrepancy in years with significant wetland flooding (Parker et al., 2018). Because surface water maps exclude most under-canopy inundation, evasion from these inundated regions may also play an important role in explaining emissions from seasonally dynamic temperate forested areas that are not reproduced in existing wetland models.

This study was designed to fill gaps in our understanding of how forested wetland size and temporal variation in inundation influence watershed-scale estimates of methane emissions. We combine elements from both the wetland and inland water calculation approaches described above to estimate one year of diffusive methane emissions from forested wetlands across a 347 $km^2$ mid-Atlantic Coastal Plain watershed. We use fine resolution frequent-repeat remote sensing imagery to estimate daily surface water extent at the wetland scale as inputs to field-validated semi-empirical models for calculating methane emissions. As in other studies, we assume surface water extent is a proxy for methane producing area. Results demonstrate that i) excluding inundation variability increased modeled methane emission totals by 66–105%, but ii) excluding small water bodies (< 1,000 $m^2$) reduced inundation estimates by 30% and subsequent emissions by 38–51%.

*Methods*

**Study area**

Our study site, the 347 $km^2$ Greensboro watershed, is on the Delmarva Peninsula (Maryland, USA), a low-gradient coastal plain landscape defined by poorly drained

soils and the persistence of small depressional forested wetlands surrounded by extensive ditch-drained agricultural land (Figure 1; Jones et al., 2018). Known as Delmarva Bays, these wetlands range in size from small closed canopy wetlands (<0.5 ha; similar to vernal pools in the northeast) to large open canopy wetlands (>5 ha; similar to Carolina Bays) (Phillips & Shedlock, 1993b). Typically they dry seasonally, having maximum inundation during the winter and decreasing water levels through the spring and summer due to evapotranspiration and agricultural groundwater withdrawal (Lee et al., 2020).

Draining to the Chesapeake Bay via the Choptank River, this watershed has been the focal point for extensive research (e.g., Ator & Denver, 2012). Land cover is mainly cultivated crops (50.5%), woody wetlands (31.5%), and deciduous forest 7.7% (Jin et al., 2019). We define wetlands using a previously developed dataset of topographic depressions (M. K. Vanderhoof & Lang, 2017) that were derived using the Stochastic Depression Analysis Tool (Lindsay, 2016a; Wu et al., 2014) and filtered using a minimum size of 50 $m^2$ and surface water extent classified from April 2015 Worldview 3 imagery (M. K. Vanderhoof et al., 2018). Polygons generally co-occur with features in the National Wetlands Inventory but they are more numerous, cover less total area, and are more spatially aligned with surface water extent. We subset this dataset to only those within woody wetlands land cover using the 2016 National Land Cover Database (Jin et al., 2019). This approach resulted in 5,118 forested wetland depressions (46% of those in the watershed), which we refer to as focal wetlands.

### Remote sensing for surface water classification

Daily time series of surface water extent for each focal wetland were calculated using 3 m resolution PlanetScope imagery (Figure 2.1; Planet, 2018). We downloaded 421 PlanetScope 4-band Analytic OrthoScenes that overlapped the study watershed and had less than 1% cloud cover. These were taken across 98 days in the 2018 water year, during which wetland surface water levels were monitored in the field. All images were Surface Reflectance products, which were atmospherically corrected using the 6SV2.1 radiative transfer model (Planet, 2018; Vermote et al., 1997). Images were masked to exclude low quality pixels indicated by the unusable data mask provided with each image. Then, we calculated a suite of spectral indices from the four bands in each image, including Normalized Difference Water Index (McFeeters, 1996), Normalized Difference Vegetation Index (Tucker, 1979), saturation, luminescence, and chroma (Zeileis et al., 2019), resulting in 9 variables for each pixel.

Training data for surface water and non-water classes were based on the National Wetlands Inventory, the 2016 National Land Cover Database, and the wetland depressions dataset developed by (M. Vanderhoof et al., 2018). We defined surface water as Freshwater Pond (n = 655) and Lake (n = 1) classes in the National Wetlands Inventory, which are classified as permanently (99%) or semi-permanently (1%) flooded. We defined non-water areas using the National Land Cover Database's forest and forested wetland classes minus pixels falling within 10 m of any National

Wetlands Inventory polygons or topographic depressions. For each image, pixel values for the 9 bands in the training regions were extracted and a random sample was used to train a random forest model that was then applied to the image. To select the best model for each image, up to 500 models were trained using random discrete sampling of a hyperparameter tuning grid varying the number of trees, which variables were sampled at each level, minimum node size, and sample rate. The model with the highest area under the precision-recall curve was selected as the best model for that image. Model performance was evaluated using internal model error statistics as well as comparisons with surface water extent calculated independently from field water level data (which was not used in model training).

For each classified image, we extracted pixel values within a 10 m buffer around each focal wetland to calculate the predicted inundation area (Figure 2.2b). We used the buffer to account for the 10 m geolocation uncertainty in the optical data (Planet, 2018), as well as potential expansion of inundation beyond topographic spill points, as is common in this landscape (Jones et al., 2018b). Where buffering resulted in overlaps between nearby polygons, any pixels that were classified as surface water were allocated to the wetland with the nearest centroid. Images that provided less than 90% coverage of the area of any wetland were excluded from its time series. Average time between usable images of each focal wetland was 6 days, resulting in a time series with 50-102 predictions across the year for each focal wetland. Average maximum time between consecutive usable images was 32 days but ranged up to 74 days. We converted the irregularly spaced predictions into a daily time series for each

focal wetland using a 50-day rolling median. Time series with gaps longer than 50 days (1%) were excluded from total inundated surface area.

### Field measurements

For comparison to areal extent of surface water estimated from remote sensing imagery, surface water extent was measured in the field at 6 wetlands in the study region (Figure 2.1). Water level was monitored in surface water wells at each wetland center using pressure transducers (Onset HOBO U20L level loggers) recording every 15 minutes. We calculated a daily time series of inundation extent for each wetland using binary classification of a 1 m LiDAR-based digital elevation model (Lang et al., 2012) using mean daily water level with a raster-based approach similar to Jones et al., (2018). Estimates were validated using monthly observations of water extent along a fixed transect at each wetland as well as surveys around the perimeter of maximum observed inundation extent in mid-March 2018.

### Methane emissions model

Daily diffusive methane emissions were calculated using wetland-specific flux rates and predicted daily surface water extent time series from the random forest classification models (Figure 2.2c). We developed three models (hereafter referred to as models A, B and C) using variations of a semi-empirical flux rate equation based on the synthesized global dataset of methane concentrations described by Holgerson and Raymond (2016) and validated with field measurements at 6 wetlands in the study area (described in the following section). Model A predicted daily flux rates by

sampling the lognormal distribution of the appropriate logarithmic size class for each wetland. For models B and C, daily flux rates for each wetland [n] were determined using Equation 2.1 with daily air temperature and atmospheric pressure from a nearby weather station to calculate gas exchange rates and equilibration concentrations of 1.85 ppm atmospheric methane for each day [i] (Winslow et al., 2016):

$$Flux_{n,i} = k_{n,i} \times \left(C_{aq[n]} - C_{eq[i]}\right) \text{ (Equation 2.1)}$$

$C_{aq[n]}$ is a time-invariant methane concentration for each wetland [n] based on its size. Gas exchange rates were calculated using daily temperature values and the size-class specific $k_{600}$ values described in Holgerson and Raymond (2016).

For model B, $C_{aq}[n]$ was randomly sampled from a lognormal distribution based on the size class of each focal wetland's original area, and for model C, $C_{aq}[n]$ was predicted from the area-concentration regression model. Because forested wetlands are a high outlier for methane on the relationship between water body size and methane concentration reported by Holgerson and Raymond (2016), our calculated emissions are likely a conservative estimate. We estimated flux rate uncertainty using Monte Carlo resampling to generate a distribution of emission estimates for each wetland by running each model 1,000 times. Cumulative annual emissions across all wetlands were calculated using Equation 2, where SWE[n,i] is the surface water extent of depression [n] on day [i] calculated from the classification model time series:

$$Total\ Emissions = \sum\sum Flux_{n,i} \times SWE_{n,i} \text{ (Equation 2.2)}$$

We evaluated the effects of different model assumptions by calculating total annual methane emissions under each model with and without changes in surface water extent, based on the original area of each focal wetland. Models accounting for changes in surface water extent we call dynamic area models; models not accounting for these we call static area models.

### Methane emissions model validation using field measurements

Methane flux rates from aquatic systems are characterized by a great deal of uncertainty, with variability often exceeding the average value of observations. The modeling approach used in this study used the best available data synthesis in the literature (Holgerson & Raymond, 2016a), which showed that some degree of variability in dissolved methane concentrations may be explained by the size of the water body. Summary statistics of concentrations and flux rates are reported for 7 logarithmic size classes. The most relevant for the present study are the two smallest size classes (<0.001 $km^2$ and 0.001-0.01 $km^2$), which account for 75% and 23% respectively of the focal wetlands and consequently comprise the majority of emissions in modeling results (Table 2.1).

We used monthly measurements of methane concentrations and flux rates collected described in Chapter 1 to validate our modeling approach. Flux rates were calculated using a combination of 24-hour static chamber incubations and the turbulent boundary layer method (i.e. based on dissolved gas measurements). For the latter, gas transfer velocities calculated from wind speed and thermal convection were validated with floating chamber incubations. Measurements were collected monthly over the

2018 water year. These wetlands were all topographic depressions that overlap with the definition of focal wetlands in this study. They generally fell into the smallest size category, or just above the threshold into the second smallest size class at just over 1,000 $m^2$. Although there was not a relationship between size and methane concentrations or fluxes among the wetlands we studied, the magnitude and range of their values were in line with the distributions reported in Holgerson and Raymond (2016). The two largest sites (1,716 $m^2$ and 1,016 $m^2$) did not have significantly lower concentrations or flux rates than the smallest size class sites, however for all sites average flux rates fell within the 95% confidence intervals of the Monte Carlo estimates of modeled flux rates with all three modeling approaches (A, B, C). Average concentrations measured in the field (Table 2.2) fell within 1 standard deviation of the mean for distributions in Table 2.1 for 5 of the 6 sites. One site in the second smallest size class receives surface inflow from a ditch and had concentrations in line with the smallest size class. Overall, this comparison shows that the magnitude and range of methane fluxes used in our modeling approach is a reasonable representation of diffusive flux rates from forested wetlands in our study region.

*Results*

**Magnitude and variability of predicted surface water extent**

Total predicted surface water extent within focal forested wetlands across the watershed ranged from a low of 1.3 $km^2$ in late July to 6.2 $km^2$ in early April, with an average of 3.75 $km^2$. This area was an order of magnitude higher than maximum extent reported for the watershed in the global surface water area database (0.70 $km^2$;

(Pekel et al., 2016b)) and represents 2.5-5.7% of the entire watershed area, 50-113% of the area of topographic depressions, and 10-23% of the total area of National Wetlands Inventory palustrine wetlands (U. S. Fish and Wildlife Service, 2019).

### Classification model performance

Classification models were sufficiently able to discriminate between water and non-water areas. Internal model performance statistics indicated a good ability to discriminate between water and non-water training regions, especially based on differences in the near-infrared band (780-860 nm). Variable importance scores indicated that the near-infrared band, along with Normalized Difference Vegetation Index and Normalized Difference Water Index, were the most informative predictors, on average accounting for 20-30% of variability between pixel values in upland and water training regions. The area under the precision-recall curve averaged 0.96 (range 0.833 to 0.99), with the lowest values for images collected between November 2017 and January 2018. Root mean square error averaged 0.263 and ranged from 0.02 to 0.42, also with the lowest accuracy in November and December 2017, and highest in spring and summer 2018.

Comparisons between field-based and satellite-based inundation time series show that our modeling approach was able to quantify the magnitude of seasonal changes in surface water extent for individual wetlands, even for those smaller than 1,000 $m^2$. For the field-monitored wetlands, the maximum predicted extent and range from classification models were significantly related to observed values ($\rho = 0.91$, $\rho =$

0.83, respectively; $\alpha = 0.05$). However, the models consistently underpredicted May and June 2018 surface water extent and overestimated November 2017 surface water extent (Figure 2.3). Monthly averaged residuals between field and satellite-based wetland areas were largest during these two periods (Figure 2.3b), but only in autumn 2017 was model accuracy also low (Figure 2.3a). The Nash-Sutcliffe criteria to evaluate model efficiency indicated poor fit (NSE <0.5) between the daily simulated and observed water extents.

### Methane emission totals under different model assumptions

Calculating watershed methane emissions using a time series approach to quantify variation in surface water coverage resulted in total estimated annual emissions 49-62% lower than when static wetland sizes were used (Figure 2.4a). Using the concentration-area regression flux model (C) resulted in higher emission totals than either the size category flux (A) or size category concentration (B) models, but in all three cases the difference between the dynamic and static models was substantially greater than variability associated with methane flux rate uncertainty. We also observed that small wetlands (< 1 ha) were responsible for a considerable proportion of modeled emissions. Although the static area models overestimated emissions for any given minimum wetland size threshold, they are only overestimates compared to the best estimate of total emissions if wetlands smaller than 1,000 $m^2$ are included. Excluding these resulted in an underestimate of total emissions by at least 10% and excluding wetlands smaller than 0.01 $km^2$ underestimated emissions by at least 75% (Figure 2.4b).

*Discussion*

We demonstrate that accounting for inundation and variable surface water extent in forested wetlands significantly influences calculations of diffusive methane emissions from a low-relief wetland-rich watershed. Specifically, we show that: i) previous limitations in quantifying surface water extent at the global scale will typically result in underestimates of methane emissions from forested wetlands; ii) as spatial resolution of wetland map products improve, accurate estimates of emissions will require improved quantification of intra-annual surface water dynamics; and iii) while fine-resolution frequent-revisit satellite imagery can help address these gaps, our ability to detect and monitor sub-canopy inundation during the late growing season is still limited. Below we discuss modeling inundation dynamics in forested wetlands and implications for the global methane budget in more detail.

### Modeling inundation dynamics of forested wetlands using high resolution satellite data

This study shows that it is possible to quantify intra-annual surface water dynamics in small forested wetlands (< 1,000 $m^2$) using optical satellite data that has both fine spatial and high temporal resolution. Although classification models were able to produce inundation time series with similar patterns to the field-based time series (Figure 2.3), they also had consistent inaccuracies, demonstrating that optical imagery alone does not accurately represent the timing of surface water dynamics in forested wetlands, especially after leaf-out.

In fall 2017, satellite-derived surface water extent was overestimated compared to our field measurements. We hypothesize this is attributable to unreliable classification of "permanent" water features in the National Wetlands Inventory, i.e. many of these water bodies are actually seasonal. Few alternatives exist for accurate training data at spatial resolutions necessary to identify the smallest water bodies, and quantitative information on hydrologic regimes is even less common. Even though the National Wetlands Inventory is very detailed and thematically rich, it has known inaccuracies in the Delmarva region (Fenstermacher et al., 2014b). Whereas variability in radiometry between Planet images required using image-specific models in this study, data from a more consistent sensor constellation (e.g., Claverie et al., 2018) could potentially be used with a more universal classification model based only on training data from time points and locations where inundation status is known with more certainty. However, seasonal and event-driven patterns of suspended sediment, chlorophyll *a*, and dissolved carbon (Hosen et al., 2018a) could affect the optical properties of these water bodies in ways that would impact model reliability.

In 2018, underestimates of surface water area in May and June coincided with the timing of canopy leaf-out. We hypothesize that underestimates are attributable to the lag between structural change in the forest canopy and the subsequent regional contraction of surface water extent (Figure 2.3a; Fisher et al., 2010; Lee et al., 2019). Canopy cover developing above areas that remain flooded, such as on the periphery of wetland depressions, obscures surface water in optical imagery. Improved methods

for inundation detection under forest canopies may be possible using synthetic aperture radar (Lang et al., 2008; Lang & Kasischke, 2008), combinations of optical and Lidar intensity data (Lang et al 2020), or improved integration with field monitoring and hydrologic models that account for upland topographic depressions (Evenson et al., 2018). While long-wavelength synthetic aperture radar sensors have been shown to be sensitive to under-canopy inundation in forested wetlands (Arnesen et al., 2013; Xaypraseuth et al., 2015), these data are not yet publicly available. Future satellite missions like the NASA-ISRO SAR (NISAR) mission, planned for launch in 2022, will provide repeat long-wavelength synthetic aperture radar imagery and thus play an important role in improving estimates of surface water dynamics in forested wetlands.

### Implications for upscaling methane emissions

As field studies continue to document high concentrations of methane in aquatic ecosystems previously overlooked as sources of emissions (Bastviken et al., 2011; Stanley et al., 2015), inventory-based emission estimates of global freshwater methane fluxes have become larger, more uncertain, and more at odds with top-down estimates in the global methane budget (Saunois et al., 2020b). Our results show that for a given set of water bodies, inventory-based emission estimates can be too high in areas where inundation extent fluctuates on a seasonal basis. However, non-permanent water bodies are also likely to be underrepresented in surface water products or mis-classified in existing landcover products due to their small size and/or obscuration by forest cover. Because the highest resolution global surface water

dataset is based on non-mixed 30 m pixels (Pekel et al., 2016b), water bodies < ~1,000 $m^2$ will be absent. At this threshold, the opposing effects of inundation dynamics and missing hidden/cryptic water bodies were of similar magnitude and resulted in a 10% underestimate of annual totals.

Understanding the source of methane is important for mitigation strategies and policies aimed at reducing carbon emissions from local to global scales. Traditional upscaling approaches for greenhouse gas emissions from freshwaters can be misleading for determining the dominant factors driving emissions (DelSontro et al., 2018a). Our results suggest that for the Greensboro watershed, the water level drawdown in natural forested wetlands considerably reduces methane producing areas. Where forested wetlands are lost and replaced with wetlands without a similar hydroperiod, such as many wetland mitigation projects (e.g., created ponds) that result in a net increase in total surface area (Dahl, 2011a), methane emissions are likely to be higher. Farm ponds and other small artificial water bodies have also been shown to have higher methane emissions on a per-area basis (Grinham et al., 2018b; Ollivier et al., 2019), and a relatively constant water level only exacerbates this difference because natural wetlands have reduced surface water extent during the warmest months when methane production rates could be the highest. The ability to detect and monitor under-canopy inundation should improve with new space-borne longer wavelength synthetic aperture radar (Arnesen et al., 2013; Xaypraseuth et al., 2015); as these capabilities improve accurately quantifying ecosystem functions of forested wetlands will also require information at high temporal resolution. Future

studies may leverage these improved technologies to better understand the role forested wetlands are playing in regional and global methane cycles by more accurately quantifying the hydrologic processes underlying methane flux to the atmosphere from inland waters.

Table 2.1. Characteristics of methane concentration and flux distributions from Holgerson and Raymond (2016) for each water body size class and the representation of size classes within the forested wetlands dataset used in this study.

| Size class ($km^2$) | Concentration Mean (sd) | Flux Mean (sd) | Fraction of focal wetlands (count) | Fraction of focal wetlands area |
|---|---|---|---|---|
| **<0.001** | 7.57 (11.60) | 2.28 (3.6) | 75% (3,850) | 17% |
| **0.001 – 0.01** | 1.70 (2.19) | 0.65 (0.72) | 23% (1,157) | 48% |
| **0.01 – 0.1** | 0.68 (0.83) | 0.28 (0.46) | 2% (109) | 32% |
| **0.1 – 1** | 0.36 (0.65) | 0.16 (0.37) | 0% (2) | 3% |

Table 2.2. Average methane concentrations and fluxes measured in 6 forested wetlands within the study region. N indicates the number of concentration measurements made at each site.

| Wetland | Size category | N | Concentration Mean (sd) | Flux Mean (sd) |
|---|---|---|---|---|
| **W1** | <0.001 $km^2$ | 8 | 14.7 (9.8) | 1.98 (1.32) |
| **W2** | <0.001 $km^2$ | 9 | 7.57 (9.1) | 1.02 (1.23) |
| **W3** | <0.001 $km^2$ | 8 | 3.05 (1.9) | 0.41 (0.26) |
| **W4** | <0.001 $km^2$ | 10 | 22.0 (22.9) | 2.97 (3.09) |
| **W5** | 0.001 – 0.01 $km^2$ | 10 | 2.84 (2.63) | 0.38 (0.35) |
| **W6** | 0.001 – 0.01 $km^2$ | 9 | 16.8 (21.2) | 2.27 (2.86) |

**Figure 2.1**. Study area showing location of the Greensboro watershed and forested wetlands. Wetland boundaries, monitoring locations, and surface water classification model predictions for 2 images are shown over corresponding color-corrected PlanetScope Visual Ortho Scenes (Planet, 2018).

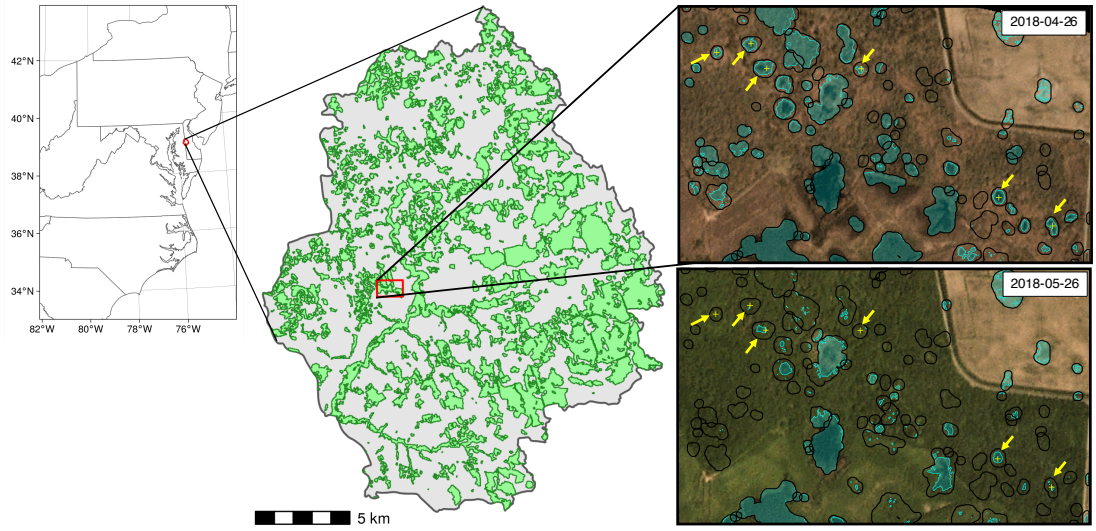

**Figure 2.2**. Image classification and emissions model workflow. **a)** Image-specific supervised classification models developed using original 4 bands (R, G, B, NIR) and derived indices NDVI, NDWI, saturation, chroma, and luminesce; **b)** Daily surface water time series derived for each focal wetland from predicted surface water area within each polygon boundary across all images; **c)** Methane emissions for each wetland (n) on day (i) derived using semi-empirical models to produce annual estimates of basin-wide emissions

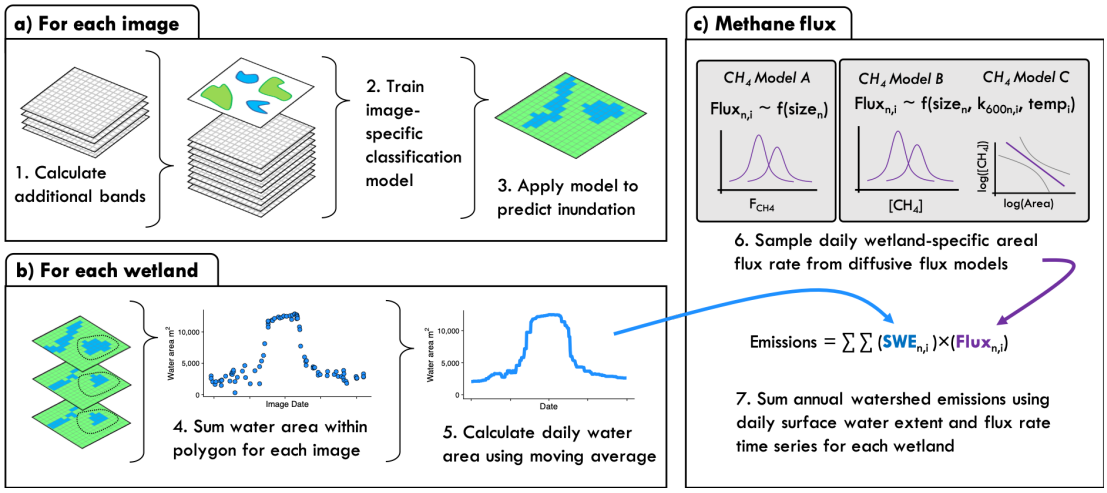

**Figure 2.3**: Comparison between inundation time series developed from field monitoring and satellite data. a) Inundation time series from two wetlands comparing field data and predictions from image-based classification models, along with estimates from individual images (points) shaded by model error rate. b) Average monthly residuals (± sd) between model predictions of SWE from image classification and field data for all observations across the 6 wetlands with field water level data

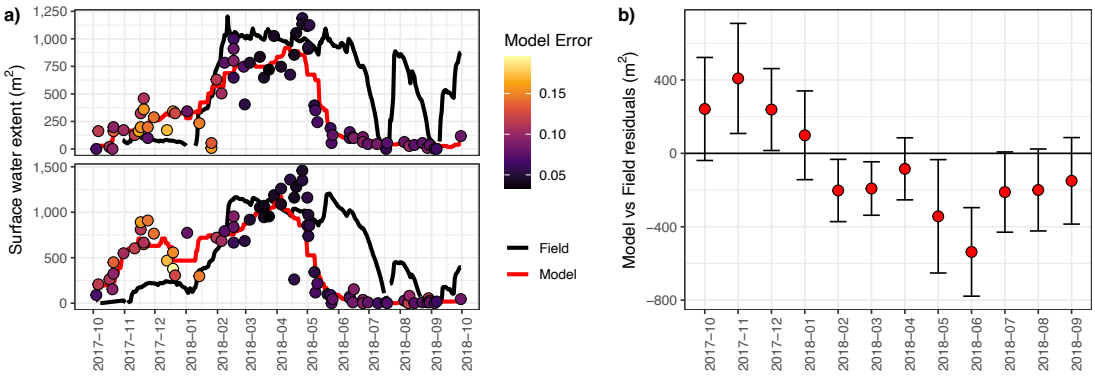

**Figure 2.4**: Total annual diffusive methane emissions for focal wetlands calculated using different model assumptions. a) Total emissions for time-varying (blue) vs. static (orange) estimates of SWE using the 3 semi-empirical diffusive flux models described in Section 2.4. Error bars represent 5% and 95% quantiles from 1,000 model iterations. b) Total emissions for time-varying vs. static SWE with different minimum wetland size thresholds.

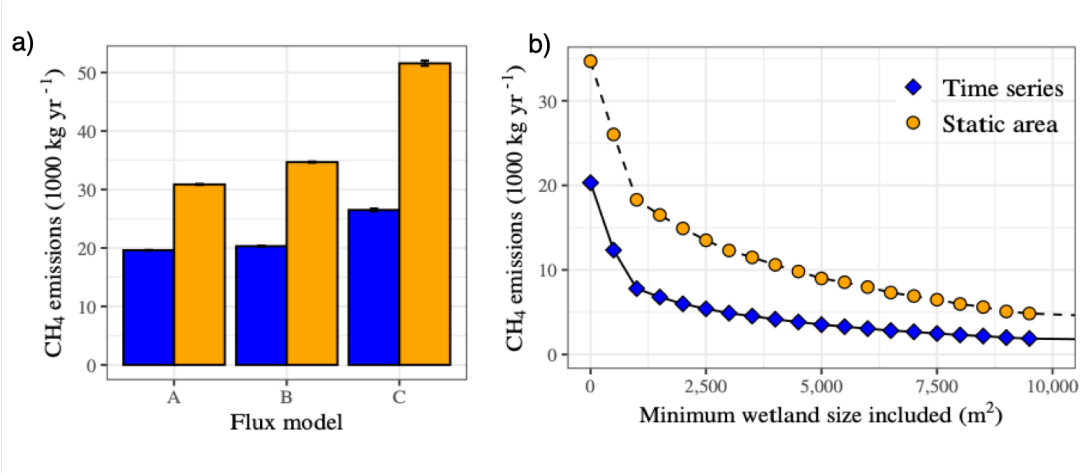

# Chapter 3: Quantifying hydrologic fluxes of dissolved methane from headwater wetlands

*Motivation*

The net climate impacts of wetland restoration remain uncertain due to continued documentation of high methane emissions in many restored wetlands (Hemes et al., 2018; Ojanen & Minkkinen, 2020; Treby et al., 2020). Whereas wetlands impacted by drainage are susceptible to losing soil carbon as carbon dioxide, reversing those impacts by increasing water storage capacity can provide favorable conditions for high rates of methane production (Badiou et al., 2011). Current methods for evaluating this tradeoff focus on comparing greenhouse gas emissions with accretion of soil carbon (Mitsch et al., 2013). However, this approach typically overlooks hydrologically mediated fluxes—including transport of dissolved methane out of wetlands in runoff and drainage channels. Although methane is a small portion of aquatic carbon budgets (Drake et al., 2018; Kindler et al., 2011), it plays a disproportionate role in net radiative forcing and is therefore particularly important for evaluating effectiveness of widely used forms of wetland restoration.

Flow modification in the form of dams or beaver structures has been shown to increase methane emissions as well as downstream dissolved methane concentrations (Crawford et al., 2016; Guérin et al., 2006; Lazar et al., 2014); however, hydrologic fluxes are not typically included in assessing the net carbon balance of restored wetlands. When lateral fluxes are included, they are generally quantified with much

less detail, including simplifying assumptions about the water budget (e.g. assuming no exchange with groundwater), and using measures of dissolved carbon that exclude volatile forms (Chu et al., 2015; D′Acunha et al., 2019; S.-C. Lee et al., 2017). However, wetland outflows may also contain dissolved methane, which can be transported downstream and evaded to the atmosphere far from its source (Figure 3.1). Increasing the potential for that methane to be oxidized or consumed instead of evaded could have measurable benefits on a wetland's net radiative forcing. Conversely, failing to account for the hydrologic export of this methane as a sink for wetland carbon may underestimate baseline levels of greenhouse gas production, ultimately limiting our ability to evaluate the net effectiveness of wetland restoration and emissions mitigation.

Studies in recent years have made significant advancements in quantifying, modeling, and mapping the nature of hydrologic connectivity between headwater wetlands and downstream waters (Golden et al., 2014; Jones et al., 2019; McLaughlin et al., 2019; Wu et al., 2019); however, we are only beginning to understand the ecological and biogeochemical significance of those connections, e.g. for the transport of dissolved gases (Cohen et al., 2016). Many headwater wetlands have natural or man-made surface channel outlets that provide hydrologic connections to the stream network at least seasonally or intermittently (Epting et al., 2018; Hosen et al., 2018b), and recent studies suggest that wetlands can be reliable sources of methane to perennial streams, especially during periods of high hydrologic connectivity (Abril & Borges, 2019; Aho & Raymond, 2019). How much of the total wetland-derived methane is advected

downstream will depend on flow conditions and geomorphic factors that control gas exchange in stream channels (Raymond et al., 2012). Some studies show that streams can completely outgas most carbon inputs from groundwater within tens or a few hundred meters of soil-stream interfaces (Kuhn et al., 2017; Maurice et al., 2017; Rocher-Ros et al., 2019), while others suggest that methane can travel dozens of kilometers downstream in low-gradient systems before evasion (Abril et al., 2014; Harms et al., 2020).

Determining if hydrologic fluxes of dissolved methane are important for assessing wetland restoration outcomes depends on (1) whether the magnitude of that flux comprises a substantial portion of a wetland's total methane output, and (2) whether wetland-derived methane that would have otherwise reached the stream network has a different fate (i.e. storage or oxidation to carbon dioxide) after restoration. Here, we present a framework for quantifying hydrologic fluxes of dissolved methane in the context of wetland restoration practices that are commonly employed in low-gradient, coastal plain landscapes (De Steven & Gramling, 2012; Jones et al., 2018a). These techniques "plug ditches" to rehydrate legacy wetlands previously drained for agriculture or mosquito control with the aim of restoring natural wetland flow regimes.

*Conceptual framework*

We define the total methane output from a wetland as the sum of atmospheric evasion from the wetland ($F_{CH_4-atm}$) plus the hydrologic flux of dissolved methane out of the wetland ($F_{CH_4-aq}$):

$$F_{CH_4} = F_{CH_4-atm} + F_{CH_4-aq} \text{ (Equation 3.1)}$$

Hydrologic flux of dissolved methane $F_{CH_4-aq}$ (mg day$^{-1}$) is defined as the product of surface water methane concentration ($CH_4$) and wetland discharge ($Q_{out}$):

$$F_{CH_4-aq} = Q_{out} \times CH_4. \text{ (Equation 3.2)}$$

We limit our focus to surface waters where, compared to subsurface flowpaths, there is less of a probability that methane is microbially processed and converted to $CO_2$ before evasion (Rasilo et al., 2017). Areal flux rates of atmospheric evasion $F_{CH_4-atm}$ (mg m$^{-2}$ day$^{-1}$) can be calculated with the turbulent boundary layer method (Cole et al., 2010) using a gas exchange rate $k$ (m day$^{-1}$), and the difference between surface water and air-equilibrated ($CH_{4eq}$) dissolved gas concentrations:

$$F_{CH_4-atm} = k \times \left(CH_4 - CH_{4eq}\right). \quad \text{(Equation 3.3)}$$

To compare these fluxes in the same units (mg day$^{-1}$), $F_{CH_4-atm}$ is multiplied by the methane-producing area ($A$, m$^2$) of the upstream wetland or catchment. We also define $\varphi_{aq}$ (unitless) as the hydrologic portion of total methane output:

$$\varphi_{aq} = \frac{F_{CH_4-aq}}{F_{CH_4-aq}+\left(F_{CH_4-atm}\times A\right)}. \text{ (Equation 3.4)}$$

Finally, we determine how far wetland-derived methane can travel in surface channels before being off-gassed using a one-dimensional linear advection model (Abril et al., 2014; Aho & Raymond, 2019). This model simulates evasion using a

flux model based on gas transfer and partial pressure differences between stream water and atmospheric equilibrium, and advection using flow velocity.

*Application to a headwater wetland catchment*

**Approach overview**

We applied this framework to estimate $F_{CH_4-aq}$ and $\varphi_{aq}$ for a headwater wetland catchment in a heavily modified low-gradient wetland-dominated landscape in the mid-Atlantic coastal plain, where much of the landscape has been drained for agriculture and ongoing restoration efforts seek to increase water tables and storage capacity (Fenstermacher et al., 2014a; M. Vanderhoof et al., 2020). Many of the remaining wetlands experience spill-fill hydrology, i.e. the wetlands fill until they reach their water storage capacity and can then spill to downgradient areas (Evenson et al., 2018; Jones et al., 2018a). Some of these channels connect headwater forested wetland complexes to the perennial stream network between approximately December and July (a staggered effect of reduced evapotranspiration), depending on catchment topography and drainage density (Epting et al., 2018), making this an ideal landscape for investigating the potential role of $F_{CH_4-aq}$ in transporting wetland methane.

We measured methane concentrations in wetland surface water with the headspace equilibrium method (Goodman, 2018; Magen et al., 2014) and calculated $Q_{out}$ using stage measurements and a 90° v-notch weir installed in an intermittent channel ~5m downstream of the wetland outlet. Topographic analysis indicates the catchment is

approximately 42.5 ha and the wetland depression drains an area of approximately 0.56 ha with a maximum inundated area less than 0.2 ha (2,000 $m^2$). Daily estimates of surface water extent were used as proxies for methane-producing areas of the upstream wetland sub-catchment and catchment (Hondula et al., 2021). We calculated daily, seasonal, and annual $\varphi_{aq}$ for both the wetland and catchment scale over a 3-year period (2018-2020) using both a high and low estimate for $k$. We ran the advection model over the same time period using one-minute timesteps and inputs over a range of parameter space representative of the landscape, which were determined from a 1 m digital elevation model and a hand-edited stream networked developed for the region (M. Vanderhoof et al., 2018). See the section at end of this chapter ("Detailed methodology") for additional information.

### Magnitude and variability of hydrologic methane flux

Model results show that for wetlands with surface water outflow channels, hydrologic export can comprise substantial portions of wetland produced methane. This contribution was highly dependent on flow status and assumptions about gas exchange, but on rare high-flow occasions the amount of dissolved methane in hydrologic fluxes could exceed gaseous methane evasion from the upstream wetland (i.e., $\varphi_{aq} > 50\%$) and account for ~20% of catchment export. The outflow channel recorded intermittent flow between 134 (37%) and 259 (71%) days each year, with annual runoff ranging between 26 and 36% of precipitation (Figure 3.2). Daily $F_{CH_4-aq}$ ranged up to 1.15 g/day, which we estimated to be up to 76% of total daily wetland $F_{CH_4}$ ($\varphi_{aq} \leq 76\%$) and up to 25% of daily catchment $F_{CH_4}$. Annual $F_{CH_4-aq}$

ranged between 21-41 g, which accounted for 23-37% total $F_{CH_4}$ from the upstream wetland and between 3-5% of $F_{CH_4}$ from the entire catchment. $\varphi_{aq}$ at both the catchment and wetland scale was generally very low (<2%) in summer and fall when there was lack of flow, except in 2020 which had a relatively wet summer (Figure 3.3). Using a high gas exchange rate for $F_{CH_4-atm}$ reduced $\varphi_{aq}$ to at most 38% and 6% at daily sub-catchment and catchment scales respectively, and 6-10% and 1% at annual sub-catchment and catchment scales. Sampling daily $CH_4$ from a uniform distribution rather than a lognormal distribution increased $F_{CH_4-aq}$ estimates up to 1.62 g $day^{-1}$ and 32-62 g $yr^{-1}$.

Transport model results indicate that only for streams with the highest slopes in this landscape will a parcel of water off-gas the majority of its methane before reaching the stream network (Figure 3.4). Slope had a large influence of the distance wetland-derived dissolved methane traveled, with notable variations at the lowest velocities. A high percentage of initial methane concentrations remained over the distances between wetland depressions and the stream network in this landscape (<400m). For slopes more gradual than the mean value estimated in this landscape, more than ~60% of the initial methane was estimated to remain in the stream after 400km. An exception is at the combination of the lowest velocities (and highest slopes), where the model estimates that 50% of the methane is lost within < 150 m.

*Implications for methane emissions mitigation*

Our results suggest that hydrologic fluxes of dissolved methane can comprise a substantial portion of wetland methane output. Because drainage channels—the conduits for $F_{CH_4-aq}$—are often directly modified by restoration projects to reverse the impacts of drainage (De Steven & Gramling, 2012), a better understanding of the magnitude and variability of $F_{CH_4-aq}$ is needed to inform ongoing efforts to operationalize accounting protocols for carbon emissions mitigation in aquatic systems (Anderson et al., 2016; Rosentreter et al., 2021). Studies comparing greenhouse gas emissions before and after hydrologic restoration that do not account for $F_{CH_4-aq}$ may be under-estimating pre-restoration emission totals and therefore risk mis-interpreting the net climate impacts of restoration efforts. Interestingly, $F_{CH_4-aq}$ and $\varphi_{aq}$ were typically highest during non-growing seasons and periods of high discharge, which are periods generally associated with lower wetland methane emissions (Hondula, Jones, et al., 2021; Melloh & Crill, 1996).

Other recent studies have demonstrated an overlooked but important role of lateral hydrologic fluxes in determining net ecosystem carbon balances (Webb et al., 2019). For example, D'Acunha et al (2019) found that including the dissolved organic carbon in drainage from a restored wetland during the non-growing season increased estimates of the wetland's carbon export by 21% on top of eddy covariance-based estimates. Because flow regime changes can also affect emissions indirectly through effects on plant productivity and composition (Cooper et al., 2014; Vanselow-Algan et al., 2015), it is important that changes to $F_{CH_4-aq}$ must be interpreted alongside

other changes to total $F_{CH_4}$. Additionally, although we assumed $CH_4$ to be chemostatic with flow conditions, studies have shown that methane concentrations can be highest during high flow conditions (Aho & Raymond, 2019; Blackburn & Stanley, 2021), making it more important to include this pathway even if surface flows are only seasonal or episodic (Epting et al., 2018).

Overall, data suggest a need to integrate lentic and lotic perspectives on greenhouse gas emissions from headwater freshwater ecosystems where systems are well-connected across terrestrial-aquatic interfaces. Methane concentrations in wetland surface waters of our study area range over two orders of magnitude (0.5-70 umol $L^{-1}$; Hondula, Jones, et al., 2021), similar to values reported for streams in southern Sweden (Wallin et al., 2014), urban/stormwater ponds (Peacock et al., 2019), and permafrost thaw ponds (Kuhn et al., 2018; Laurion et al., 2010; Polishchuk et al., 2018). These values are high compared to average concentrations in streams (Stanley et al 2016), so if even a portion of this methane makes it to the downstream network it would result in local hotspots in streams. In the Upper Choptank river watershed, approximately half of the wetland depressions can be connected to the stream network during wet years (M. Vanderhoof et al., 2018), with a maximum distance between wetland depressions and stream network less than 500 m (M. Vanderhoof et al., 2016). Much of the methane produced in wetland soils has the potential to reach that perennial stream network, which means it may be off-gassed far from its source and importantly, potentially outside the measurement footprint of gas sensors monitoring an upstream wetland. Data from flux towers with large footprints that

include ditches suggest these features have an outsized influence on emissions (Desai et al., 2015); however, it is unclear what proportion of gases are produced in ditches versus advected in runoff from drained upland systems (Romeijn et al., 2019). This also has implications for efforts to upscale emissions from ditch networks. Because drainage from wetland areas may be a source contributing to the high methane concentrations found in ditches (Peacock et al., 2021), lateral advection may need to be accounted for to upscale emissions from ditch networks. Better mapping of intermittent stream channels and ditches, as well as the geomorphic characteristics necessary to model gas exchange (e.g. slope), will enable predictions about the location and magnitude of elevated methane concentrations in river networks based on connectivity of upstream wetlands, in order to help prioritize emission mitigation efforts.

Assessing wetland carbon balances, especially in the context of restoration, will undoubtedly involve many uncertainties and necessary simplifying assumptions. Our results suggest that lateral exports of dissolved methane—which are usually not explicitly quantified in wetland carbon budgets—may be substantial enough to merit inclusion. We recommend that wetland and landscape carbon budgets consider potential changes to lateral fluxes of dissolved methane and other greenhouse gases when discussing net impacts of hydrologic restoration, especially for projects that alter drainage patterns and those with climate mitigation goals.

*Detailed methodology*

Lateral dissolved methane fluxes ($F_{CH_4-aq}$) were calculated from measurements of dissolved gas concentrations ($CH_4$) and a discharge time series ($Q_{out}$). Dissolved methane concentrations were calculated from with samples collected monthly in triplicate near the center of the main wetland, and twice during the study period for each of twenty nearby wetlands. Atmospheric gas sample were collected for site- and date-specific headspace calculations. Headspace gas was transferred into evacuated vials (Labco, UK), and analyzed using a gas chromatograph (SRI 8610C).

Discharge was calculated using a 90º v-notch weir installed in an intermittent channel ~5m downstream of the wetland outlet. Stage at the weir was estimated using a correlation between instantaneous measurements of flow and wetland stage. Wetland stage was measured at 15-minute intervals using pressure transducers (HOBO water level data loggers) installed in a shallow well close to the center of the wetland and barometric from a dry well installed ~ 10 m from the wetland. The 15-minute time series was aggregated to calculate daily water volume flowing out of the wetland catchment. Discharge was corrected for artificially high periods of runoff, likely due to the presence of woody debris and leaves that impounded water at the wetland outflow. Daily methane export was calculated as the product of daily water volume and methane concentrations sampled from either a lognormal or uniform distribution fit to the measured values, using the average of 1,000 model iterations.

Daily estimates of atmospheric evasion ($F_{CH_4-atm}$) from the upstream wetland and catchment area were calculated as the product of an areal flux rate and daily estimates of surface water extent, which is a useful proxy for methane emissions source area for wetlands without emergent vegetation in this landscape (Hondula, Jones, et al., 2021). Flux rates were calculated assuming only diffusive emissions using the turbulent boundary layer model, using the same dissolved methane concentration used to estimate lateral export, at both a high (0.72 m $day^{-1}$) and low (0.14 m $day^{-1}$) gas exchange rate for small forested wetlands (Holgerson et al., 2017). Catchment (42,445 $m^2$) and wetland sub-catchment (5,602 $m^2$) areas were delineated from a 1-m digital elevation model using Whitebox (Lindsay, 2016b). A stage-area curve was developed for both the wetland sub-catchment and watershed, which were used to estimate surface water area (i.e. methane source area). As a conservative estimate for calculating the importance of hydrologic fluxes (i.e. maximizing $F_{CH_4-atm}$ relative to $F_{CH_4-aq}$), the minimum surface water extent was used for days when water level was below the wetland spill point and there was no discharge in the intermittent channel. In reality, the surface water extent contracts further and may even disappear during low water levels during mid to late growing season. However, this reduction in area is difficult to quantify accurately and coincides with the warmest months when $F_{CH_4-atm}$ may therefore be highest. We compared the total amount of methane leaving both the wetland and catchment via evasion and hydrologic export over daily, seasonal, and annual timescales over a 3-year period (2018-2020).

To determine how far wetland-derived methane might travel in surface channels before being lost to the atmosphere, we used a one-dimensional linear advection model (Abril et al., 2014). This model simulates evasion using a flux model based on gas transfer and partial pressure differences between stream water and atmospheric equilibration. We ran the model using one-minute timesteps and inputs over a range of parameter space representative of the shallow topography and flow conditions in the study area. Gas exchange coefficients were calculated from slope and velocity (Raymond et al., 2012). Slope from wetlands to stream network was based on a 1m digital elevation map using depressions and hand-edited stream network developed for the region (M. Vanderhoof et al., 2017). We calculated a distribution of slopes using the elevation difference between each depression and its nearest lower elevation stream segment.

**Figure 3.1**: Conceptual diagram representing fates of wetland-derived methane in a drained (left) and restored (right) wetland landscape. Vertical arrows indicate atmospheric evasion from standing surface water (smaller from the drained wetland) and horizontal arrows indicate the flux of dissolved methane in flowing water (larger from the drained wetland).

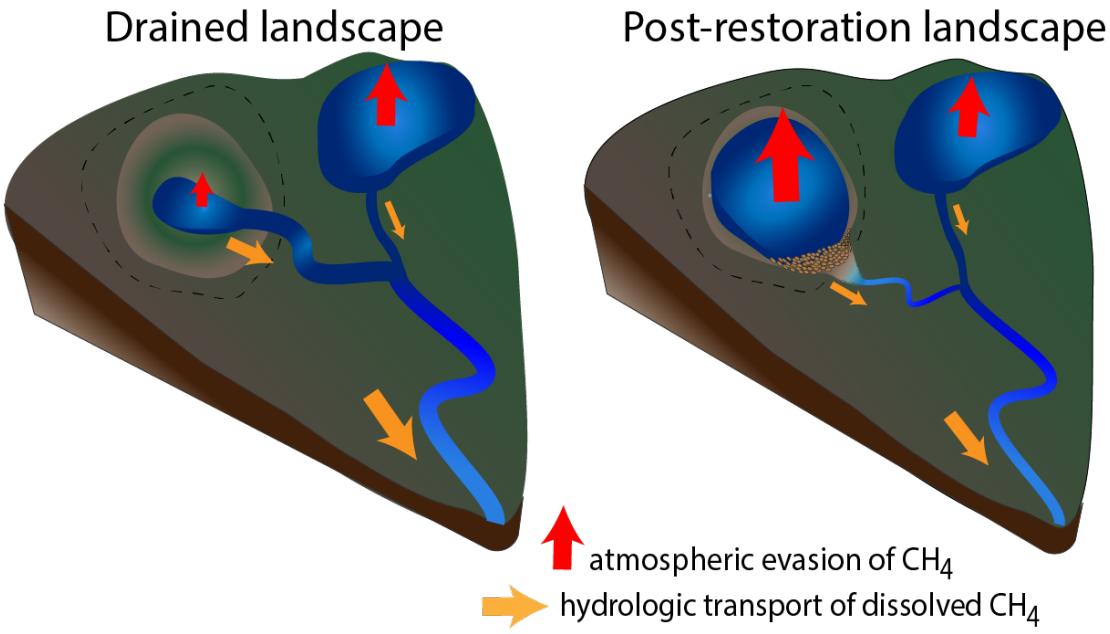

**Figure 3.2**. Daily wetland discharge and estimated cumulative annual hydrologic methane flux.

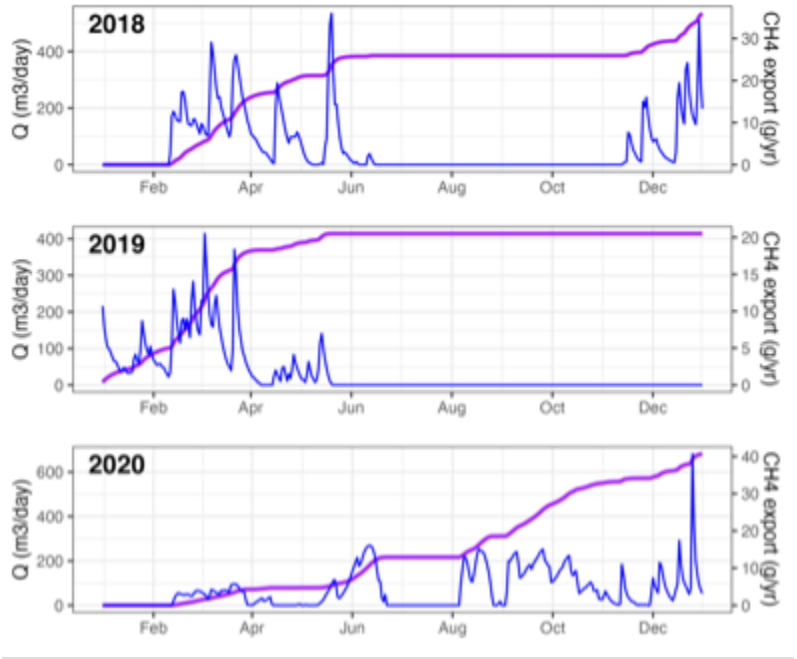

**Figure 3.3**. Hydrologic export as proportion of total methane output at catchment (left) and wetland sub-catchment (right) scales by season. Values indicate range between estimates calculated with a high and low gas exchange rate (k).

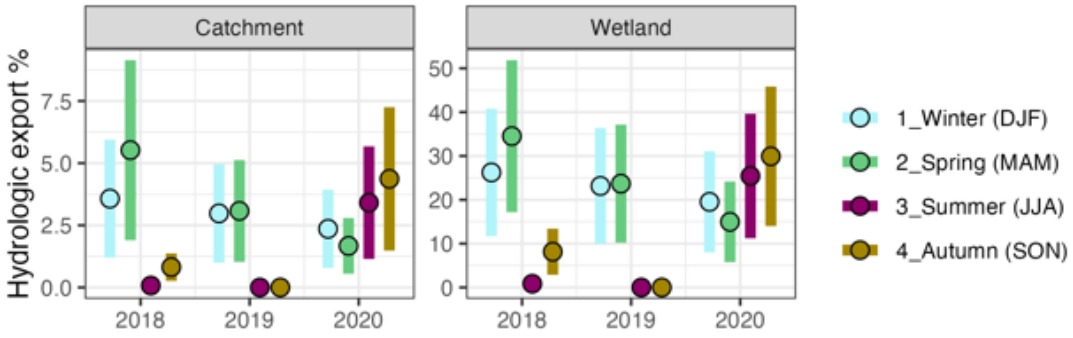

**Figure 3.4**. Transport model results showing percent of methane remaining after (a) 100m, (b) 400m, (c) 1km of downstream transport. Red line indicates average slope between wetland depressions and nearest stream.

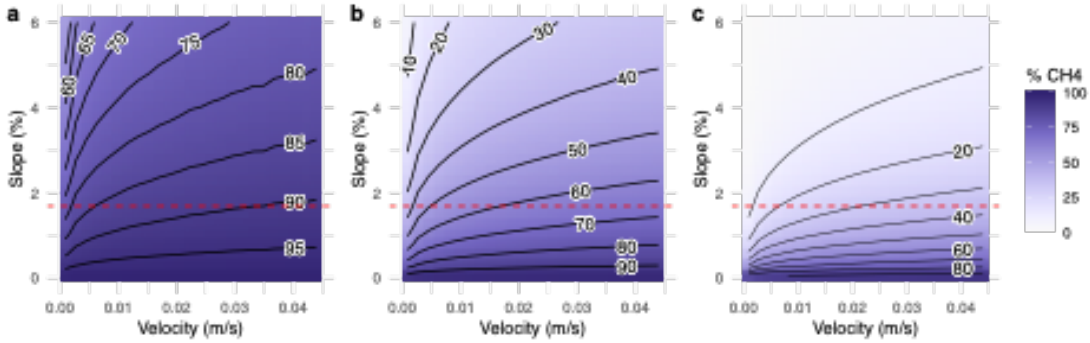

# Summary and Conclusions

In this dissertation, I studied the relationship between wetland hydrology and methane emissions in seasonal freshwater forested wetlands. To accomplish this, I studied the magnitude and variability of methane fluxes from hydrologic gradients at six wetlands. I monitored water levels in order to quantify time series of wetland inundation and surface water extent, and used statistical models to evaluate the relationship between hydrologic variables and methane flux rates. I also analyzed satellite images with machine learning models to quantify inundation time series, and compared those results to field-based inundation time series. I used the results of the machine learning models to quantify the influence of model assumptions on the calculation of total wetland methane emissions for the Greensboro watershed. Finally, I developed a conceptual framework for quantifying hydrologic fluxes of dissolved methane out of wetlands, a pathway that is currently overlooked in assessments of wetland restoration.

In Chapter 1, I show that there is a non-linear relationship between water levels and methane flux rates in forested mineral soil wetlands. Methane fluxes were dramatically higher from inundated compared to non-inundated soils, and the direction of water level changes helped explain variability in the magnitude of flux rates. Intermittently inundated soils alternated between being sources and sinks of methane depending on hydrologic conditions. Using field measurements in four different upscaling models showed that a time series of surface water extent was a valid proxy for wetland methane producing area. Current trends in the coverage of

wetland types in US show large declines of forested wetlands and gains in wetland types with more stable water levels such as farm ponds and created wetlands. These results imply that this trend could be leading to higher net methane emissions from wetlands.

In Chapter 2, I show that commonly used methods for quantifying surface water extent result in underestimates of inundation and methane emissions from forested wetlands, and therefore new methods are needed to accurately detect and monitor inundation dynamics in forested wetlands. Surface water classification using 3 m optical imagery identified an order of magnitude more surface water than the maximum extent reported in the global surface water database, but is limited by reliable training data of small water bodies as well as occlusion of sub-canopy inundation. Results show that upscaling methane emissions from small water bodies will require data on surface water extent at both higher spatial and temporal resolutions than is currently used.

In Chapter 3, I develop and apply a framework for quantifying hydrologic fluxes of dissolved methane from headwater wetlands. I explain why they are a relevant but missing component of current approaches to the assessment of net carbon balances in wetlands, and why there is a need to integrate perspectives from wetland and stream scientists. Results from empirical modeling show that hydrologic fluxes can comprise a substantial portion of wetland methane output, and that drainage channels can transport much of this methane to downstream perennial waters.

Freshwater wetlands and other small water bodies are one of the largest sources of methane to the atmosphere. Recent increases in the rate of global methane emissions may be attributable in large part to increased inundation extent and duration in natural and man-made wetlands. This research indicates that the natural hydrologic regime of forested wetlands plays a role in limiting their total methane emissions, but new techniques are needed in order to detect and monitor these patterns at global scales. Models for upscaling methane emissions from the smallest size class water bodies will need to account for intra-annual inundation variability and hydrologic fluxes, especially for predicting changes to methane emissions associated with land cover change, management and restoration activities, and increased variability in precipitation rates.

# Bibliography


Abril, G., & Borges, A. V. (2019). Ideas and perspectives: Carbon leaks from flooded land: do we need to replumb the inland water active pipe? *Biogeosciences*, *16*(3), 769–784. https://doi.org/10.5194/bg-16-769-2019

Abril, G., Martinez, J.-M., Artigas, L. F., Moreira-Turcq, P., Benedetti, M. F., Vidal, L., Meziane, T., Kim, J.-H., Bernardes, M. C., Savoye, N., Deborde, J., Souza, E. L., Albéric, P., Landim de Souza, M. F., & Roland, F. (2014). Amazon River carbon dioxide outgassing fuelled by wetlands. *Nature*, *505*(7483), 395–398. https://doi.org/10.1038/nature12797

Aho, K. S., & Raymond, P. A. (2019). Differential Response of Greenhouse Gas Evasion to Storms in Forested and Wetland Streams. *Journal of Geophysical Research: Biogeosciences*, *124*(3), 649–662. https://doi.org/10.1029/2018JG004750

Allen, G. H., & Pavelsky, T. M. (2018). Global extent of rivers and streams. *Science*, *361*(6402), 585–588. https://doi.org/10.1126/science.aat0636

Altor, A. E., & Mitsch, W. J. (2008). Pulsing hydrology, methane emissions and carbon dioxide fluxes in created marshes: A 2-year ecosystem study. *Wetlands*, *28*(2), 423–438. https://doi.org/10.1672/07-98.1

Anderson, F. E., Bergamaschi, B., Sturtevant, C., Knox, S., Hastings, L., Windham-Myers, L., Detto, M., Hestir, E. L., Drexler, J., Miller, R. L., Matthes, J. H., Verfaillie, J., Baldocchi, D., Snyder, R. L., & Fujii, R. (2016). Variation of energy and carbon fluxes from a restored temperate freshwater wetland and implications for carbon market verification protocols. *Journal of Geophysical Research: Biogeosciences*, *121*(3), 777–795. https://doi.org/10.1002/2015JG003083

Angle, J. C., Morin, T. H., Solden, L. M., Narrowe, A. B., Smith, G. J., Borton, M. A., Rey-Sanchez, C., Daly, R. A., Mirfenderesgi, G., Hoyt, D. W., Riley, W. J., Miller, C. S., Bohrer, G., & Wrighton, K. C. (2017). Methanogenesis in oxygenated soils is a substantial fraction of wetland methane emissions. *Nature Communications*, *8*(1), 1567. https://doi.org/10.1038/s41467-017-01753-4

Arnesen, A. S., Silva, T. S. F., Hess, L. L., Novo, E. M. L. M., Rudorff, C. M., Chapman, B. D., & McDonald, K. C. (2013). Monitoring flood extent in the lower Amazon River floodplain using ALOS/PALSAR ScanSAR images. *Remote Sensing of Environment*, *130*, 51–61. https://doi.org/10.1016/j.rse.2012.10.035

Ator, S. W., & Denver, J. M. (2012). Estimating Contributions of Nitrate and Herbicides From Groundwater to Headwater Streams, Northern Atlantic Coastal Plain, United States [1]: ESTIMATING CONTRIBUTIONS OF NITRATE AND HERBICIDES FROM GROUNDWATER TO HEADWATER STREAMS, NORTHERN ATLANTIC COASTAL PLAIN, UNITED STATES. *JAWRA Journal of the American Water Resources Association*, *48*(6), 1075–1090. https://doi.org/10.1111/j.1752-1688.2012.00672.x

Badiou, P., McDougal, R., Pennock, D., & Clark, B. (2011). Greenhouse gas emissions and carbon sequestration potential in restored wetlands of the Canadian prairie pothole region. *Wetlands Ecology and Management*, *19*(3), 237–256. https://doi.org/10.1007/s11273-011-9214-6

Bansal, S., Johnson, O. F., Meier, J., & Zhu, X. (2020). Vegetation Affects Timing and Location of Wetland Methane Emissions. *Journal of Geophysical Research: Biogeosciences*, *125*(9). https://doi.org/10.1029/2020JG005777

Bartlett, K. B., & Harriss, R. C. (1993). Review and assessment of methane emissions from wetlands. *Chemosphere*, *26*(1–4), 261–320. https://doi.org/10.1016/0045-6535(93)90427-7

Bastviken, D., Cole, J. J., Pace, M. L., & Van de Bogert, M. C. (2008). Fates of methane from different lake habitats: Connecting whole-lake budgets and CH $_4$ emissions. *Journal of Geophysical Research: Biogeosciences*, *113*(G2), n/a-n/a. https://doi.org/10.1029/2007JG000608

Bastviken, D., Cole, J., Pace, M., & Tranvik, L. (2004). Methane emissions from lakes: Dependence of lake characteristics, two regional assessments, and a global estimate. *Global Biogeochemical Cycles*, *18*(4), n/a-n/a. https://doi.org/10.1029/2004GB002238

Bastviken, D., Tranvik, L. J., Downing, J. A., Crill, P. M., & Enrich-Prast, A. (2011). Freshwater Methane Emissions Offset the Continental Carbon Sink. *Science*, *331*(6013), 50–50. https://doi.org/10.1126/science.1196808

Bhullar, G. S., Iravani, M., Edwards, P. J., & Olde Venterink, H. (2013). Methane transport and emissions from soil as affected by water table and vascular plants. *BMC Ecology*, *13*(1), 32. https://doi.org/10.1186/1472-6785-13-32

Bishop, K., Buffam, I., Erlandsson, M., Fölster, J., Laudon, H., Seibert, J., & Temnerud, J. (2008). Aqua Incognita: The unknown headwaters. *Hydrological Processes*, *22*(8), 1239–1242. https://doi.org/10.1002/hyp.7049

Blackburn, S. R., & Stanley, E. H. (2021). Floods increase carbon dioxide and methane fluxes in agricultural streams. *Freshwater Biology*, *66*(1), 62–77. https://doi.org/10.1111/fwb.13614

Bohn, T. J., Podest, E., Schroeder, R., Pinto, N., McDonald, K. C., Glagolev, M., Filippov, I., Maksyutov, S., Heimann, M., Chen, X., & Lettenmaier, D. P. (2013). Modeling the large-scale effects of surface moisture heterogeneity on wetland carbon fluxes in the West Siberian Lowland. *Biogeosciences*, *10*(10), 6559–6576. https://doi.org/10.5194/bg-10-6559-2013

Boon, P. I., & Lee, K. (1997). Methane oxidation in sediments of a floodplain wetland in south-eastern Australia. *Letters in Applied Microbiology*, *25*(2), 138–142. https://doi.org/10.1046/j.1472-765X.1997.00189.x

Bridgham, S. D., Cadillo-Quiroz, H., Keller, J. K., & Zhuang, Q. (2013). Methane emissions from wetlands: Biogeochemical, microbial, and modeling perspectives from local to global scales. *Global Change Biology*, *19*(5), 1325–1346. https://doi.org/10.1111/gcb.12131

Bridgham, S. D., Megonigal, J. P., Keller, J. K., Bliss, N. B., & Trettin, C. (2006). The carbon balance of North American wetlands. *Wetlands*, *26*(4), 889–916. https://doi.org/10.1672/0277-5212(2006)26[889:TCBONA]2.0.CO;2

Calabrese, S., Garcia, A., Wilmoth, J. L., Zhang, X., & Porporato, A. (2021). Critical inundation level for methane emissions from wetlands. *Environmental Research Letters*, *16*(4), 044038. https://doi.org/10.1088/1748-9326/abedea

Cawley, K. (2018). *NeonDissGas*. https://github.com/NEONScience/NEON-dissolved-gas

Chamberlain, S. D., Gomez-Casanovas, N., Walter, M. T., Boughton, E. H., Bernacchi, C. J., DeLucia, E. H., Groffman, P. M., Keel, E. W., & Sparks, J. P. (2016). Influence of transient flooding on methane fluxes from subtropical pastures. *Journal of Geophysical Research: Biogeosciences*, *121*(3), 965–977. https://doi.org/10.1002/2015JG003283

Chu, H., Gottgens, J. F., Chen, J., Sun, G., Desai, A. R., Ouyang, Z., Shao, C., & Czajkowski, K. (2015). Climatic variability, hydrologic anomaly, and methane emission can turn productive freshwater marshes into net carbon sources. *Global Change Biology*, *21*(3), 1165–1181. https://doi.org/10.1111/gcb.12760

Claverie, M., Ju, J., Masek, J. G., Dungan, J. L., Vermote, E. F., Roger, J.-C., Skakun, S. V., & Justice, C. (2018). The Harmonized Landsat and Sentinel-2 surface reflectance data set. *Remote Sensing of Environment*, *219*, 145–161. https://doi.org/10.1016/j.rse.2018.09.002

Cohen, M. J., Creed, I. F., Alexander, L., Basu, N. B., Calhoun, A. J. K., Craft, C., D'Amico, E., DeKeyser, E., Fowler, L., Golden, H. E., Jawitz, J. W., Kalla,

P., Kirkman, L. K., Lane, C. R., Lang, M., Leibowitz, S. G., Lewis, D. B., Marton, J., McLaughlin, D. L., … Walls, S. C. (2016). Do geographically isolated wetlands influence landscape functions? *Proceedings of the National Academy of Sciences*, *113*(8), 1978–1986. https://doi.org/10.1073/pnas.1512650113

Cole, J. J., Bade, D. L., Bastviken, D., Pace, M. L., & Van de Bogert, M. (2010). Multiple approaches to estimating air-water gas exchange in small lakes: Gas exchange in lakes. *Limnology and Oceanography: Methods*, *8*(6), 285–293. https://doi.org/10.4319/lom.2010.8.285

Cole, J. J., Prairie, Y. T., Caraco, N. F., McDowell, W. H., Tranvik, L. J., Striegl, R. G., Duarte, C. M., Kortelainen, P., Downing, J. A., Middelburg, J. J., & Melack, J. (2007). Plumbing the Global Carbon Cycle: Integrating Inland Waters into the Terrestrial Carbon Budget. *Ecosystems*, *10*(1), 172–185. https://doi.org/10.1007/s10021-006-9013-8

Cooley, S. W., Smith, L. C., Ryan, J. C., Pitcher, L. H., & Pavelsky, T. M. (2019). Arctic-Boreal lake dynamics revealed using CubeSat imagery. *Geophysical Research Letters*. https://doi.org/10.1029/2018GL081584

Cooper, Mark. D. A., Evans, Christopher. D., Zielinski, P., Levy, Peter. E., Gray, A., Peacock, M., Norris, D., Fenner, N., & Freeman, C. (2014). Infilled Ditches are Hotspots of Landscape Methane Flux Following Peatland Re-wetting. *Ecosystems*, *17*(7), 1227–1241. https://doi.org/10.1007/s10021-014-9791-3

Crawford, J. T., Loken, L. C., Stanley, E. H., Stets, E. G., Dornblaser, M. M., & Striegl, R. G. (2016). Basin scale controls on $CO_2$ and $CH_4$ emissions from the Upper Mississippi River: Mississippi River Greenhouse Gases. *Geophysical Research Letters*, *43*(5), 1973–1979. https://doi.org/10.1002/2015GL067599

D′Acunha, B., Morillas, L., Black, T. A., Christen, A., & Johnson, M. S. (2019). Net Ecosystem Carbon Balance of a Peat Bog Undergoing Restoration: Integrating $CO_2$ and $CH_4$ Fluxes From Eddy Covariance and Aquatic Evasion With DOC Drainage Fluxes. *Journal of Geophysical Research: Biogeosciences*, *124*(4), 884–901. https://doi.org/10.1029/2019JG005123

Dahl, T. E. (2011a). *Status and trends of wetlands in the conterminous United States 2004 to 2009* (p. 108). U.S. Department of the Interior; Fish and Wildlife Service.

Dahl, T. E. (2011b). *Status and Trends of Wetlands in the Conterminous US 2004 to 2009*. U.S. Department of the Interior; Fish and Wildlife Service. https://www.fws.gov/wetlands/documents/status-and-trends-of-wetlands-in-the-conterminous-united-states-2004-to-2009.pdf

Davidson, E. A., Savage, K., Verchot, L. V., & Navarro, R. (2002). Minimizing artifacts and biases in chamber-based measurements of soil respiration. *Agricultural and Forest Meteorology*, *113*(1–4), 21–37. https://doi.org/10.1016/S0168-1923(02)00100-4

De Steven, D., & Gramling, J. M. (2012). Diverse Characteristics of Wetlands Restored under the Wetlands Reserve Program in the Southeastern United States. *Wetlands*, *32*(4), 593–604. https://doi.org/10.1007/s13157-012-0303-y

DelSontro, T., Beaulieu, J. J., & Downing, J. A. (2018a). Greenhouse gas emissions from lakes and impoundments: Upscaling in the face of global change: GHG emissions from lakes and impoundments. *Limnology and Oceanography Letters*. https://doi.org/10.1002/lol2.10073

DelSontro, T., Beaulieu, J. J., & Downing, J. A. (2018b). Greenhouse gas emissions from lakes and impoundments: Upscaling in the face of global change: GHG emissions from lakes and impoundments. *Limnology and Oceanography Letters*, *3*(3), 64–75. https://doi.org/10.1002/lol2.10073

Desai, A. R., Xu, K., Tian, H., Weishampel, P., Thom, J., Baumann, D., Andrews, A. E., Cook, B. D., King, J. Y., & Kolka, R. (2015). Landscape-level terrestrial methane flux observed from a very tall tower. *Agricultural and Forest Meteorology*, *201*, 61–75. https://doi.org/10.1016/j.agrformet.2014.10.017

DeVries, B., Huang, C., Lang, M., Jones, J., Huang, W., Creed, I., & Carroll, M. (2017). Automated Quantification of Surface Water Inundation in Wetlands Using Optical Satellite Imagery. *Remote Sensing*, *9*(8), 807. https://doi.org/10.3390/rs9080807

Dewitz, J. (2019). *National Land Cover Dataset (NLCD) 2016 Products* [Data set]. U.S. Geological Survey. https://doi.org/10.5066/P96HHBIE

Downing, J. A., Prairie, Y. T., Cole, J. J., Duarte, C. M., Tranvik, L. J., Striegl, R. G., McDowell, W. H., Kortelainen, P., Caraco, N. F., Melack, J. M., & Middelburg, J. J. (2006). The global abundance and size distribution of lakes, ponds, and impoundments. *Limnology and Oceanography*, *51*(5), 2388–2397. https://doi.org/10.4319/lo.2006.51.5.2388

Drake, T. W., Raymond, P. A., & Spencer, R. G. M. (2018). Terrestrial carbon inputs to inland waters: A current synthesis of estimates and uncertainty: Terrestrial carbon inputs to inland waters. *Limnology and Oceanography Letters*, *3*(3), 132–142. https://doi.org/10.1002/lol2.10055

Dutaur, L., & Verchot, L. V. (2007). A global inventory of the soil CH $_4$ sink: A GLOBAL INVENTORY OF THE SOIL CH $_4$ SINK. *Global Biogeochemical Cycles*, *21*(4), n/a-n/a. https://doi.org/10.1029/2006GB002734

Epting, S. M., Hosen, J. D., Alexander, L. C., Lang, M. W., Armstrong, A. W., & Palmer, M. A. (2018). Landscape metrics as predictors of hydrologic connectivity between Coastal Plain forested wetlands and streams. *Hydrological Processes*, *32*(4), 516–532. https://doi.org/10.1002/hyp.11433

Estop-Aragonés, C., Knorr, K.-H., & Blodau, C. (2012). *Belowground in situ redox dynamics and methanogenesis recovery in a degraded fen during dry-wet cycles and flooding* [Preprint]. Biogeochemistry: Wetlands. https://doi.org/10.5194/bgd-9-11655-2012

Evenson, G. R., Golden, H. E., Lane, C. R., McLaughlin, D. L., & D'Amico, E. (2018). Depressional wetlands affect watershed hydrological, biogeochemical, and ecological functions. *Ecological Applications*, *28*(4), 953–966. https://doi.org/10.1002/eap.1701

Evenson, G. R., Jones, C. N., McLaughlin, D. L., Golden, H. E., Lane, C. R., DeVries, B., Alexander, L. C., Lang, M. W., McCarty, G. W., & Sharifi, A. (2018). A watershed-scale model for depressional wetland-rich landscapes. *Journal of Hydrology X*, *1*, 100002. https://doi.org/10.1016/j.hydroa.2018.10.002

Evenson, G. R., McLaughlin, D. L., Lane, C. R., DeVries, B., Alexander, L. C., Lang, M. W., McCarty, G. W., & Sharifi, A. (2018). A watershed-scale model for depressional wetland-rich landscapes. *Journal of Hydrology X*, *1*, 100002. https://doi.org/10.1016/j.hydroa.2018.10.002

Fenstermacher, D. E., Rabenhorst, M. C., Lang, M. W., McCarty, G. W., & Needelman, B. A. (2014a). Distribution, Morphometry, and Land Use of Delmarva Bays. *Wetlands*, *34*(6), 1219–1228. https://doi.org/10.1007/s13157-014-0583-5

Fenstermacher, D. E., Rabenhorst, M. C., Lang, M. W., McCarty, G. W., & Needelman, B. A. (2014b). Distribution, Morphometry, and Land Use of Delmarva Bays. *Wetlands*, *34*(6), 1219–1228. https://doi.org/10.1007/s13157-014-0583-5

Fest, B. J., Hinko-Najera, N., Wardlaw, T., Griffith, D. W. T., Livesley, S. J., & Arndt, S. K. (2017). Soil methane oxidation in both dry and wet temperate eucalypt forests shows a near-identical relationship with soil air-filled porosity. *Biogeosciences*, *14*(2), 467–479. https://doi.org/10.5194/bg-14-467-2017

Fisher, T., Jordan, T., Staver, K., Gustafson, A., Koskelo, A., Fox, R., Sutton, A., Kana, T., Beckert, K., Stone, J., McCarty, G., & Lang, M. (2010a). The Choptank Basin in Transition: Intensifying Agriculture, Slow Urbanization, and Estuarine Eutrophication. In M. Kennish & H. Paerl (Eds.), *Coastal Lagoons* (Vol. 20103358, pp. 135–165). CRC Press. https://doi.org/10.1201/EBK1420088304-c7

Fisher, T., Jordan, T., Staver, K., Gustafson, A., Koskelo, A., Fox, R., Sutton, A., Kana, T., Beckert, K., Stone, J., McCarty, G., & Lang, M. (2010b). The Choptank Basin in Transition: Intensifying Agriculture, Slow Urbanization, and Estuarine Eutrophication. In M. Kennish & H. Paerl (Eds.), *Coastal Lagoons* (Vol. 20103358, pp. 135–165). CRC Press. https://doi.org/10.1201/EBK1420088304-c7

Gatland, J. R., Santos, I. R., Maher, D. T., Duncan, T. M., & Erler, D. V. (2014). Carbon dioxide and methane emissions from an artificially drained coastal wetland during a flood: Implications for wetland global warming potential. *Journal of Geophysical Research: Biogeosciences*, *119*(8), 1698–1716. https://doi.org/10.1002/2013JG002544

Golden, H. E., Lane, C. R., Amatya, D. M., Bandilla, K. W., Raanan Kiperwas, H., Knightes, C. D., & Ssegane, H. (2014). Hydrologic connectivity between geographically isolated wetlands and surface water systems: A review of select modeling methods. *Environmental Modelling & Software*, *53*, 190–206. https://doi.org/10.1016/j.envsoft.2013.12.004

Golladay, S. W., Clayton, B. A., Brantley, S. T., Smith, C. R., Qi, J., & Hicks, D. W. (2021). Forest restoration increases isolated wetland hydroperiod: A long-term case study. *Ecosphere*, *12*(5). https://doi.org/10.1002/ecs2.3495

Goodman, K. (2018). *AOS Protocol and Procedure: Surface Water Dissolved Gas Sampling* (NEON.DOC.001199). https://data.neonscience.org/documents/10179/2093436/NEON.DOC.001199vL/f58f5422-2c1e-489b-ba12-97048fe7414c

Griffin, C. G., McClelland, J. W., Frey, K. E., Fiske, G., & Holmes, R. M. (2018). Quantifying CDOM and DOC in major Arctic rivers during ice-free conditions using Landsat TM and ETM+ data. *Remote Sensing of Environment*, *209*, 395–409. https://doi.org/10.1016/j.rse.2018.02.060

Grinham, A., Albert, S., Deering, N., Dunbabin, M., Bastviken, D., Sherman, B., Lovelock, C. E., & Evans, C. D. (2018a). The importance of small artificial water bodies as sources of methane emissions in Queensland, Australia. *Hydrology and Earth System Sciences*, *22*(10), 5281–5298. https://doi.org/10.5194/hess-22-5281-2018

Grinham, A., Albert, S., Deering, N., Dunbabin, M., Bastviken, D., Sherman, B., Lovelock, C. E., & Evans, C. D. (2018b). The importance of small artificial water bodies as sources of methane emissions in Queensland, Australia. *Hydrology and Earth System Sciences*, *22*(10), 5281–5298. https://doi.org/10.5194/hess-22-5281-2018

Grossart, H.-P., Frindte, K., Dziallas, C., Eckert, W., & Tang, K. W. (2011). Microbial methane production in oxygenated water column of an oligotrophic lake. *Proceedings of the National Academy of Sciences*, *108*(49), 19657–19661. https://doi.org/10.1073/pnas.1110716108

Guérin, F., Abril, G., Richard, S., Burban, B., Reynouard, C., Seyler, P., & Delmas, R. (2006). Methane and carbon dioxide emissions from tropical reservoirs: Significance of downstream rivers. *Geophysical Research Letters*, *33*(21), L21407. https://doi.org/10.1029/2006GL027929

Halabisky, M., Moskal, L. M., Gillespie, A., & Hannam, M. (2016). Reconstructing semi-arid wetland surface water dynamics through spectral mixture analysis of a time series of Landsat satellite images (1984–2011). *Remote Sensing of Environment*, *177*, 171–183. https://doi.org/10.1016/j.rse.2016.02.040

Hanson, P. C., Carpenter, S. R., Cardille, J. A., Coe, M. T., & Winslow, L. A. (2007). Small lakes dominate a random sample of regional lake characteristics. *Freshwater Biology*, *52*(5), 814–822. https://doi.org/10.1111/j.1365-2427.2007.01730.x

Happell, J. D., Chanton, J. P., & Showers, W. J. (1995). Methane transfer across the water-air interface in stagnant wooded swamps of Florida: Evaluation of mass-transfer coefficients and isotropic fractionation. *Limnology and Oceanography*, *40*(2), 290–298. https://doi.org/10.4319/lo.1995.40.2.0290

Harms, T. K., Rocher-Ros, G., & Godsey, S. E. (2020). Emission of Greenhouse Gases From Water Tracks Draining Arctic Hillslopes. *Journal of Geophysical Research: Biogeosciences*, *125*(12). https://doi.org/10.1029/2020JG005889

Hayashi, M., van der Kamp, G., & Rosenberry, D. O. (2016). Hydrology of Prairie Wetlands: Understanding the Integrated Surface-Water and Groundwater Processes. *Wetlands*, *36*(S2), 237–254. https://doi.org/10.1007/s13157-016-0797-9

Hemes, K. S., Chamberlain, S. D., Eichelmann, E., Knox, S. H., & Baldocchi, D. D. (2018). A Biogeochemical Compromise: The High Methane Cost of Sequestering Carbon in Restored Wetlands. *Geophysical Research Letters*, *45*(12), 6081–6091. https://doi.org/10.1029/2018GL077747

Hendriks, D. M. D., van Huissteden, J., & Dolman, A. J. (2010). Multi-technique assessment of spatial and temporal variability of methane fluxes in a peat meadow. *Agricultural and Forest Meteorology*, *150*(6), 757–774. https://doi.org/10.1016/j.agrformet.2009.06.017

Herbst, M., Friborg, T., Ringgaard, R., & Soegaard, H. (2011). Interpreting the variations in atmospheric methane fluxes observed above a restored wetland. *Agricultural and Forest Meteorology*, *151*(7), 841–853. https://doi.org/10.1016/j.agrformet.2011.02.002

Holgerson, M. A., Farr, E. R., & Raymond, P. A. (2017). Gas transfer velocities in small forested ponds. *Journal of Geophysical Research: Biogeosciences*, *122*(5), 1011–1021. https://doi.org/10.1002/2016JG003734

Holgerson, M. A., & Raymond, P. A. (2016a). Large contribution to inland water CO2 and CH4 emissions from very small ponds. *Nature Geoscience*, *9*(3), 222–226. https://doi.org/10.1038/ngeo2654

Holgerson, M. A., & Raymond, P. A. (2016b). Large contribution to inland water CO2 and CH4 emissions from very small ponds. *Nature Geoscience*, *9*(3), 222–226. https://doi.org/10.1038/ngeo2654

Hondula, K. L., DeVries, B., Jones, C. N., & Palmer, M. A. (2021). Effects of Using High Resolution Satellite-based Inundation Time Series to Estimate Methane Fluxes from Forested Wetlands. *Geophysical Research Letters*. https://doi.org/10.1029/2021GL092556

Hondula, K. L., Jones, C. N., & Palmer, M. A. (2021). Effects of seasonal inundation on methane fluxes from forested freshwater wetlands. *Environmental Research Letters*, *16*(8), 084016. https://doi.org/10.1088/1748-9326/ac1193

Hosen, J. D., Armstrong, A. W., & Palmer, M. A. (2018a). Dissolved organic matter variations in coastal plain wetland watersheds: The integrated role of hydrological connectivity, land use, and seasonality. *Hydrological Processes*, *32*(11), 1664–1681. https://doi.org/10.1002/hyp.11519

Hosen, J. D., Armstrong, A. W., & Palmer, M. A. (2018b). Dissolved organic matter variations in coastal plain wetland watersheds: The integrated role of hydrological connectivity, land use, and seasonality. *Hydrological Processes*, *32*(11), 1664–1681. https://doi.org/10.1002/hyp.11519

Huang, C., Peng, Y., Lang, M., Yeo, I.-Y., & McCarty, G. (2014a). Wetland inundation mapping and change monitoring using Landsat and airborne LiDAR data. *Remote Sensing of Environment*, *141*, 231–242. https://doi.org/10.1016/j.rse.2013.10.020

Huang, C., Peng, Y., Lang, M., Yeo, I.-Y., & McCarty, G. (2014b). Wetland inundation mapping and change monitoring using Landsat and airborne LiDAR data. *Remote Sensing of Environment*, *141*, 231–242. https://doi.org/10.1016/j.rse.2013.10.020

Jeffrey, L. C., Maher, D. T., Johnston, S. G., Maguire, K., Steven, A. D. L., & Tait, D. R. (2019). Rhizosphere to the atmosphere: Contrasting methane pathways, fluxes, and geochemical drivers across the terrestrial–aquatic wetland boundary. *Biogeosciences*, *16*(8), 1799–1815. https://doi.org/10.5194/bg-16-1799-2019

Ji, L., Zhang, L., & Wylie, B. (2009). Analysis of Dynamic Thresholds for the Normalized Difference Water Index. *Photogrammetric Engineering & Remote Sensing*, *75*(11), 1307–1317. https://doi.org/10.14358/PERS.75.11.1307

Jia, K., Jiang, W., Li, J., & Tang, Z. (2018). Spectral matching based on discrete particle swarm optimization: A new method for terrestrial water body extraction using multi-temporal Landsat 8 images. *Remote Sensing of Environment*, *209*, 1–18. https://doi.org/10.1016/j.rse.2018.02.012

Jin, S., Homer, C., Yang, L., Danielson, P., Dewitz, J., Li, C., Zhu, Z., Xian, G., & Howard, D. (2019). Overall Methodology Design for the United States National Land Cover Database 2016 Products. *Remote Sensing*, *11*(24), 2971. https://doi.org/10.3390/rs11242971

Jones, C. N., Ameli, A., Neff, B. P., Evenson, G. R., McLaughlin, D. L., Golden, H. E., & Lane, C. R. (2019). Modeling Connectivity of Non-floodplain Wetlands: Insights, Approaches, and Recommendations. *JAWRA Journal of the American Water Resources Association*, *55*(3), 559–577. https://doi.org/10.1111/1752-1688.12735

Jones, C. N., Evenson, G. R., McLaughlin, D. L., Vanderhoof, M. K., Lang, M. W., McCarty, G. W., Golden, H. E., Lane, C. R., & Alexander, L. C. (2018a). Estimating restorable wetland water storage at landscape scales. *Hydrological Processes*, *32*(2), 305–313. https://doi.org/10.1002/hyp.11405

Jones, C. N., Evenson, G. R., McLaughlin, D. L., Vanderhoof, M. K., Lang, M. W., McCarty, G. W., Golden, H. E., Lane, C. R., & Alexander, L. C. (2018b). Estimating restorable wetland water storage at landscape scales. *Hydrological Processes*, *32*(2), 305–313. https://doi.org/10.1002/hyp.11405

Jungkunst, H. F., & Fiedler, S. (2007). Latitudinal differentiated water table control of carbon dioxide, methane and nitrous oxide fluxes from hydromorphic soils: Feedbacks to climate change. *Global Change Biology*, *13*(12), 2668–2683. https://doi.org/10.1111/j.1365-2486.2007.01459.x

Kannenberg, S. A., Dunn, S. T., Ludwig, S. M., Spawn, S. A., & Schade, J. D. (2015). Patterns of Potential Methanogenesis Along Soil Moisture Gradients Following Drying and Rewetting in Midwestern Prairie Pothole Wetlands. *Wetlands*, *35*(4), 633–640. https://doi.org/10.1007/s13157-015-0653-3

Keiluweit, M., Wanzek, T., Kleber, M., Nico, P., & Fendorf, S. (2017). Anaerobic microsites have an unaccounted role in soil carbon stabilization. *Nature Communications*, *8*(1), 1771. https://doi.org/10.1038/s41467-017-01406-6

Kim, D.-G., Vargas, R., Bond-Lamberty, B., & Turetsky, M. R. (2012). Effects of soil rewetting and thawing on soil gas fluxes: A review of current literature and suggestions for future research. *Biogeosciences*, *9*(7), 2459–2483. https://doi.org/10.5194/bg-9-2459-2012

Kindler, R., Siemens, J., Kaiser, K., Walmsley, D. C., Bernhofer, C., Buchmann, N., Cellier, P., Eugster, W., Gleixner, G., Grũnwald, T., Heim, A., Ibrom, A., Jones, S. K., Jones, M., Klumpp, K., Kutsch, W., Larsen, K. S., Lehuger, S., Loubet, B., … Kaupenjohann, M. (2011). Dissolved carbon leaching from soil is a crucial component of the net ecosystem carbon balance: DISSOLVED CARBON LEACHING. *Global Change Biology*, *17*(2), 1167–1185. https://doi.org/10.1111/j.1365-2486.2010.02282.x

Knorr, K.-H., Lischeid, G., & Blodau, C. (2009). Dynamics of redox processes in a minerotrophic fen exposed to a water table manipulation. *Geoderma*, *153*(3–4), 379–392. https://doi.org/10.1016/j.geoderma.2009.08.023

Knox, S. H., Bansal, S., McNicol, G., Schafer, K., Sturtevant, C., Ueyama, M., Valach, A. C., Baldocchi, D., Delwiche, K., Desai, A. R., Euskirchen, E., Liu, J., Lohila, A., Malhotra, A., Melling, L., Riley, W., Runkle, B. R. K., Turner, J., Vargas, R., … Jackson, R. B. (2021). Identifying dominant environmental predictors of freshwater wetland methane fluxes across diurnal to seasonal time scales. *Global Change Biology*, gcb.15661. https://doi.org/10.1111/gcb.15661

Kuhn, C., Bettigole, C., Glick, H. B., Seegmiller, L., Oliver, C. D., & Raymond, P. (2017). Patterns in stream greenhouse gas dynamics from mountains to plains in northcentral Wyoming. *Journal of Geophysical Research*, 18.

Kuhn, C., de Matos Valerio, A., Ward, N., Loken, L., Sawakuchi, H. O., Kampel, M., Richey, J., Stadler, P., Crawford, J., Striegl, R., Vermote, E., Pahlevan, N., & Butman, D. (2019). Performance of Landsat-8 and Sentinel-2 surface reflectance products for river remote sensing retrievals of chlorophyll-a and turbidity. *Remote Sensing of Environment*, *224*, 104–118. https://doi.org/10.1016/j.rse.2019.01.023

Lang, M., McDonough, O., McCarty, G., Oesterling, R., & Wilen, B. (2012). Enhanced Detection of Wetland-Stream Connectivity Using LiDAR. *Wetlands*, *32*(3), 461–473. https://doi.org/10.1007/s13157-012-0279-7

Lang, M., Stedman, S.-M., Nettles, J., & Griffin, R. (2020). Coastal Watershed Forested Wetland Change and Opportunities for Enhanced Collaboration with the Forestry Community. *Wetlands*, *40*(1), 7–19. https://doi.org/10.1007/s13157-019-01243-x

Lang, M. W., & Kasischke, E. S. (2008). Using C-Band Synthetic Aperture Radar Data to Monitor Forested Wetland Hydrology in Maryland's Coastal Plain, USA. *IEEE Transactions on Geoscience and Remote Sensing*, *46*(2), 535–546. https://doi.org/10.1109/TGRS.2007.909950

Lang, M. W., Kasischke, E. S., Prince, S. D., & Pittman, K. W. (2008). Assessment of C-band synthetic aperture radar data for mapping and monitoring Coastal Plain forested wetlands in the Mid-Atlantic Region, U.S.A. *Remote Sensing of Environment*, *112*(11), 4120–4130. https://doi.org/10.1016/j.rse.2007.08.026

Lang, M. W., Kim, V., McCarty, G. W., Li, X., Yeo, I.-Y., Huang, C., & Du, L. (2020). Improved Detection of Inundation below the Forest Canopy using Normalized LiDAR Intensity Data. *Remote Sensing*, *12*(4), 707. https://doi.org/10.3390/rs12040707

Lang, McDonough, O., McCarty, G., Oesterling, R., & Wilen, B. (2012). Enhanced Detection of Wetland-Stream Connectivity Using LiDAR. *Wetlands*, *32*(3), 461–473. https://doi.org/10.1007/s13157-012-0279-7

Lazar, J. G., Addy, K., Welsh, M. K., Gold, A. J., & Groffman, P. M. (2014). Resurgent Beaver Ponds in the Northeastern United States: Implications for Greenhouse Gas Emissions. *Journal of Environmental Quality*, *43*(6), 1844–1852. https://doi.org/10.2134/jeq2014.02.0065

Le Mer, J., & Roger, P. (2001). Production, oxidation, emission and consumption of methane by soils: A review. *European Journal of Soil Biology*, *37*(1), 25–50. https://doi.org/10.1016/S1164-5563(01)01067-6

Lee, McCarty, G. W., Moglen, G. E., Lang, M. W., Nathan Jones, C., Palmer, M., Yeo, I.-Y., Anderson, M., Sadeghi, A. M., & Rabenhorst, M. C. (2020). Seasonal drivers of geographically isolated wetland hydrology in a low-gradient, Coastal Plain landscape. *Journal of Hydrology*, *583*, 124608. https://doi.org/10.1016/j.jhydrol.2020.124608

Lee, S., Yeo, I.-Y., Lang, M. W., McCarty, G. W., Sadeghi, A. M., Sharifi, A., Jin, H., & Liu, Y. (2019). Improving the catchment scale wetland modeling using

remotely sensed data. *Environmental Modelling & Software*, *122*, 104069. https://doi.org/10.1016/j.envsoft.2017.11.001

Lee, S.-C., Christen, A., Black, A. T., Johnson, M. S., Jassal, R. S., Ketler, R., Nesic, Z., & Merkens, M. (2017). Annual greenhouse gas budget for a bog ecosystem undergoing restoration by rewetting. *Biogeosciences*, *14*(11), 2799–2814. https://doi.org/10.5194/bg-14-2799-2017

Lee, Yeo, I.-Y., Lang, M. W., McCarty, G. W., Sadeghi, A. M., Sharifi, A., Jin, H., & Liu, Y. (2019). Improving the catchment scale wetland modeling using remotely sensed data. *Environmental Modelling & Software*, *122*, 104069. https://doi.org/10.1016/j.envsoft.2017.11.001

Lindsay, J. B. (2016a). Whitebox GAT: A case study in geomorphometric analysis. *Computers & Geosciences*, *95*, 75–84. https://doi.org/10.1016/j.cageo.2016.07.003

Lindsay, J. B. (2016b). Whitebox GAT: A case study in geomorphometric analysis. *Computers & Geosciences*, *95*, 75–84. https://doi.org/10.1016/j.cageo.2016.07.003

Lohila, A., Aalto, T., Aurela, M., Hatakka, J., Tuovinen, J., Kilkki, J., Penttilä, T., Vuorenmaa, J., Hänninen, P., Sutinen, R., Viisanen, Y., & Laurila, T. (2016). Large contribution of boreal upland forest soils to a catchment-scale $CH_4$ balance in a wet year. *Geophysical Research Letters*, *43*(6), 2946–2953. https://doi.org/10.1002/2016GL067718

Lowe, W. H., & Likens, G. E. (2005). Moving Headwater Streams to the Head of the Class. *BioScience*, *55*(3), 196. https://doi.org/10.1641/0006-3568(2005)055[0196:MHSTTH]2.0.CO;2

Magen, C., Lapham, L. L., Pohlman, J. W., Marshall, K., Bosman, S., Casso, M., & Chanton, J. P. (2014). A simple headspace equilibration method for measuring dissolved methane. *Limnology and Oceanography: Methods*, *12*(9), 637–650. https://doi.org/10.4319/lom.2014.12.637

Maietta, C. E., Hondula, K. L., Jones, C. N., & Palmer, M. A. (2020). Hydrological Conditions Influence Soil and Methane-Cycling Microbial Populations in Seasonally Saturated Wetlands. *Frontiers in Environmental Science*, *8*, 593942. https://doi.org/10.3389/fenvs.2020.593942

Marcé, R., Obrador, B., Gómez-Gener, L., Catalán, N., Koschorreck, M., Arce, M. I., Singer, G., & von Schiller, D. (2019). Emissions from dry inland waters are a blind spot in the global carbon cycle. *Earth-Science Reviews*, *188*, 240–248. https://doi.org/10.1016/j.earscirev.2018.11.012

Maurice, L., Rawlins, B. G., Farr, G., Bell, R., & Gooddy, D. C. (2017). The Influence of Flow and Bed Slope on Gas Transfer in Steep Streams and Their Implications for Evasion of $CO_2$: Gas Transfer Tracer Paper. *Journal of Geophysical Research: Biogeosciences*, *122*(11), 2862–2875. https://doi.org/10.1002/2017JG004045

McFeeters, S. K. (1996). The use of the Normalized Difference Water Index (NDWI) in the delineation of open water features. *International Journal of Remote Sensing*, *17*(7), 1425–1432. https://doi.org/10.1080/01431169608948714

McLaughlin, D. L., Diamond, J. S., Quintero, C., Heffernan, J., & Cohen, M. J. (2019). Wetland Connectivity Thresholds and Flow Dynamics From Stage Measurements. *Water Resources Research*, *55*(7), 6018–6032. https://doi.org/10.1029/2018WR024652

McNamara, N. P., Chamberlain, P. M., Piearce, T. G., Sleep, D., Black, H. I. J., Reay, D. S., & Ineson, P. (2006). Impact of water table depth on forest soil methane turnover in laboratory soil cores deduced from natural abundance and tracer $^{13}$C stable isotope experiments. *Isotopes in Environmental and Health Studies*, *42*(4), 379–390. https://doi.org/10.1080/10256010600990765

Melloh, R. A., & Crill, P. M. (1996). Winter methane dynamics in a temperate peatland. *Global Biogeochemical Cycles*, *10*(2), 247–254. https://doi.org/10.1029/96GB00365

Melton, J. R., Wania, R., Hodson, E. L., Poulter, B., Ringeval, B., Spahni, R., Bohn, T., Avis, C. A., Beerling, D. J., Chen, G., Eliseev, A. V., Denisov, S. N., Hopcroft, P. O., Lettenmaier, D. P., Riley, W. J., Singarayer, J. S., Subin, Z. M., Tian, H., Zürcher, S., … Kaplan, J. O. (2013). Present state of global wetland extent and wetland methane modelling: Conclusions from a model inter-comparison project (WETCHIMP). *Biogeosciences*, *10*(2), 753–788. https://doi.org/10.5194/bg-10-753-2013

Mitsch, W. J., Bernal, B., Nahlik, A. M., Mander, Ü., Zhang, L., Anderson, C. J., Jørgensen, S. E., & Brix, H. (2013). Wetlands, carbon, and climate change. *Landscape Ecology*, *28*(4), 583–597. https://doi.org/10.1007/s10980-012-9758-8

Natchimuthu, S., Sundgren, I., Gålfalk, M., Klemedtsson, L., Crill, P., Danielsson, Å., & Bastviken, D. (2016). Spatio-temporal variability of lake $CH_4$ fluxes and its influence on annual whole lake emission estimates: Spatio-temporal lake $CH_4$ fluxes. *Limnology and Oceanography*, *61*(S1), S13–S26. https://doi.org/10.1002/lno.10222

Ojanen, P., & Minkkinen, K. (2020). Rewetting Offers Rapid Climate Benefits for Tropical and Agricultural Peatlands But Not for Forestry-Drained Peatlands. *Global Biogeochemical Cycles*, *34*(7). https://doi.org/10.1029/2019GB006503

Ollivier, Q. R., Maher, D. T., Pitfield, C., & Macreadie, P. I. (2019). Punching above their weight: Large release of greenhouse gases from small agricultural dams. *Global Change Biology*, *25*(2), 721–732. https://doi.org/10.1111/gcb.14477

Pangala, S. R., Enrich-Prast, A., Basso, L. S., Peixoto, R. B., Bastviken, D., Hornibrook, E. R. C., Gatti, L. V., Ribeiro, H., Calazans, L. S. B., Sakuragui, C. M., Bastos, W. R., Malm, O., Gloor, E., Miller, J. B., & Gauci, V. (2017). Large emissions from floodplain trees close the Amazon methane budget. *Nature*. https://doi.org/10.1038/nature24639

Parker, R. J., Boesch, H., McNorton, J., Comyn-Platt, E., Gloor, M., Wilson, C., Chipperfield, M. P., Hayman, G. D., & Bloom, A. A. (2018). Evaluating year-to-year anomalies in tropical wetland methane emissions using satellite CH4 observations. *Remote Sensing of Environment*, *211*, 261–275. https://doi.org/10.1016/j.rse.2018.02.011

Peacock, M., Audet, J., Bastviken, D., Futter, M. N., Gauci, V., Grinham, A., Harrison, J. A., Kent, M. S., Kosten, S., Lovelock, C. E., Veraart, A. J., & Evans, C. D. (2021). Global importance of methane emissions from drainage ditches and canals. *Environmental Research Letters*, *16*(4), 044010. https://doi.org/10.1088/1748-9326/abeb36

Pedersen, A. R., Petersen, S. O., & Schelde, K. (2010). A comprehensive approach to soil-atmosphere trace-gas flux estimation with static chambers. *European Journal of Soil Science*, *61*(6), 888–902. https://doi.org/10.1111/j.1365-2389.2010.01291.x

Pekel, J.-F., Cottam, A., Gorelick, N., & Belward, A. S. (2016a). High-resolution mapping of global surface water and its long-term changes. *Nature*, *540*(7633), 418–422. https://doi.org/10.1038/nature20584

Pekel, J.-F., Cottam, A., Gorelick, N., & Belward, A. S. (2016b). High-resolution mapping of global surface water and its long-term changes. *Nature*, *540*(7633), 418–422. https://doi.org/10.1038/nature20584

Peltola, O., Hensen, A., Belelli Marchesini, L., Helfter, C., Bosveld, F. C., van den Bulk, W. C. M., Haapanala, S., van Huissteden, J., Laurila, T., Lindroth, A., Nemitz, E., Röckmann, T., Vermeulen, A. T., & Mammarella, I. (2015). Studying the spatial variability of methane flux with five eddy covariance towers of varying height. *Agricultural and Forest Meteorology*, *214–215*, 456–472. https://doi.org/10.1016/j.agrformet.2015.09.007

Pennock, D., Yates, T., Bedard-Haughn, A., Phipps, K., Farrell, R., & McDougal, R. (2010). Landscape controls on N2O and CH4 emissions from freshwater mineral soil wetlands of the Canadian Prairie Pothole region. *Geoderma*, *155*(3–4), 308–319. https://doi.org/10.1016/j.geoderma.2009.12.015

Phillips, P. J., & Shedlock, R. J. (1993a). Hydrology and chemistry of groundwater and seasonal ponds in the Atlantic Coastal Plain in Delaware, USA. *Journal of Hydrology*, *141*(1–4), 157–178. https://doi.org/10.1016/0022-1694(93)90048-E

Phillips, P. J., & Shedlock, R. J. (1993b). Hydrology and chemistry of groundwater and seasonal ponds in the Atlantic Coastal Plain in Delaware, USA. *Journal of Hydrology*, *141*(1–4), 157–178. https://doi.org/10.1016/0022-1694(93)90048-E

Planet. (2018). *Planet Imagery Product Specification: Planetscope and RapidEye*. https://www.planet.com/products/satellite-imagery/files/Planet_Combined_Imagery_Product_Specs_December2017.pdf

Podgrajsek, E., Sahlée, E., & Rutgersson, A. (2014). Diurnal cycle of lake methane flux: Diurnal cycle of lake methane flux. *Journal of Geophysical Research: Biogeosciences*, *119*(3), 236–248. https://doi.org/10.1002/2013JG002327

Poindexter, C. M., Baldocchi, D. D., Matthes, J. H., Knox, S. H., & Variano, E. A. (2016). The contribution of an overlooked transport process to a wetland's methane emissions. *Geophysical Research Letters*, *43*(12), 6276–6284. https://doi.org/10.1002/2016GL068782

Poindexter, C. M., & Variano, E. A. (2013). Gas exchange in wetlands with emergent vegetation: The effects of wind and thermal convection at the air-water interface. *Journal of Geophysical Research: Biogeosciences*, *118*(3), 1297–1306. https://doi.org/10.1002/jgrg.20099

Poulter, B., Bousquet, P., Canadell, J. G., Ciais, P., Peregon, A., Saunois, M., Arora, V. K., Beerling, D. J., Brovkin, V., Jones, C. D., Joos, F., Gedney, N., Ito, A., Kleinen, T., Koven, C. D., McDonald, K., Melton, J. R., Peng, C., Peng, S., … Zhu, Q. (2017a). Global wetland contribution to 2000–2012 atmospheric methane growth rate dynamics. *Environmental Research Letters*, *12*(9), 094013. https://doi.org/10.1088/1748-9326/aa8391

Poulter, B., Bousquet, P., Canadell, J. G., Ciais, P., Peregon, A., Saunois, M., Arora, V. K., Beerling, D. J., Brovkin, V., Jones, C. D., Joos, F., Gedney, N., Ito, A., Kleinen, T., Koven, C. D., McDonald, K., Melton, J. R., Peng, C., Peng, S., … Zhu, Q. (2017b). Global wetland contribution to 2000–2012 atmospheric methane growth rate dynamics. *Environmental Research Letters*, *12*(9), 094013. https://doi.org/10.1088/1748-9326/aa8391

Rasilo, T., Hutchins, R. H. S., Ruiz-González, C., & del Giorgio, P. A. (2017). Transport and transformation of soil-derived CO2, CH4 and DOC sustain CO2 supersaturation in small boreal streams. *Science of The Total Environment*, *579*, 902–912. https://doi.org/10.1016/j.scitotenv.2016.10.187

Ratering, S., & Conrad, RalF. (1998). Effects of short-term drainage and aeration on the production of methane in submerged rice soil. *Global Change Biology*, *4*(4), 397–407. https://doi.org/10.1046/j.1365-2486.1998.00162.x

Raymond, P. A., Hartmann, J., Lauerwald, R., Sobek, S., McDonald, C., Hoover, M., Butman, D., Striegl, R., Mayorga, E., Humborg, C., Kortelainen, P., Dürr, H., Meybeck, M., Ciais, P., & Guth, P. (2013). Global carbon dioxide emissions from inland waters. *Nature*, *503*(7476), 355–359. https://doi.org/10.1038/nature12760

Raymond, P. A., Zappa, C. J., Butman, D., Bott, T. L., Potter, J., Mulholland, P., Laursen, A. E., McDowell, W. H., & Newbold, D. (2012). *Scaling the gas transfer velocity and hydraulic geometry in streams and small rivers*. 13.

Rocher-Ros, G., Sponseller, R. A., Lidberg, W., Mörth, C., & Giesler, R. (2019). Landscape process domains drive patterns of $CO_2$ evasion from river networks. *Limnology and Oceanography Letters*, *4*(4), 87–95. https://doi.org/10.1002/lol2.10108

Romeijn, P., Comer-Warner, S. A., Ullah, S., Hannah, D. M., & Krause, S. (2019). Streambed Organic Matter Controls on Carbon Dioxide and Methane Emissions from Streams. *Environmental Science & Technology*, *53*(5), 2364–2374. https://doi.org/10.1021/acs.est.8b04243

Rosentreter, J. A., Al-Haj, A. N., Fulweiler, R. W., & Williamson, P. (2021). Methane and Nitrous Oxide Emissions Complicate Coastal Blue Carbon Assessments. *Global Biogeochemical Cycles*, *35*(2). https://doi.org/10.1029/2020GB006858

Sakabe, A., Kosugi, Y., Okumi, C., Itoh, M., & Takahashi, K. (2016). Impacts of riparian wetlands on the seasonal variations of watershed-scale methane budget in a temperate monsoonal forest: Watershed-Scale $CH_4$ Budget in a Forest. *Journal of Geophysical Research: Biogeosciences*, *121*(7), 1717–1732. https://doi.org/10.1002/2015JG003292

Saunois, M., Stavert, A. R., Poulter, B., Bousquet, P., Canadell, J. G., Jackson, R. B., Raymond, P. A., Dlugokencky, E. J., Houweling, S., Patra, P. K., Ciais, P., Arora, V. K., Bastviken, D., Bergamaschi, P., Blake, D. R., Brailsford, G., Bruhwiler, L., Carlson, K. M., Carrol, M., … Zhuang, Q. (2020a). The Global

Methane Budget 2000–2017. *Earth System Science Data*, *12*(3), 1561–1623. https://doi.org/10.5194/essd-12-1561-2020

Saunois, M., Stavert, A. R., Poulter, B., Bousquet, P., Canadell, J. G., Jackson, R. B., Raymond, P. A., Dlugokencky, E. J., Houweling, S., Patra, P. K., Ciais, P., Arora, V. K., Bastviken, D., Bergamaschi, P., Blake, D. R., Brailsford, G., Bruhwiler, L., Carlson, K. M., Carrol, M., … Zhuang, Q. (2020b). The Global Methane Budget 2000–2017. *Earth System Science Data*, *12*(3), 1561–1623. https://doi.org/10.5194/essd-12-1561-2020

Seekell, D. A., Carr, J. A., Gudasz, C., & Karlsson, J. (2014). Upscaling carbon dioxide emissions from lakes: Upscaling CO2 emissions from lakes. *Geophysical Research Letters*, *41*(21), 7555–7559. https://doi.org/10.1002/2014GL061824

Sieczko, A. K., Duc, N. T., Schenk, J., Pajala, G., Rudberg, D., Sawakuchi, H. O., & Bastviken, D. (2020). Diel variability of methane emissions from lakes. *Proceedings of the National Academy of Sciences*, *117*(35), 21488–21494. https://doi.org/10.1073/pnas.2006024117

Soil Survey Staff. (2020). *Web Soil Survey*. Web Soil Survey. http://websoilsurvey.sc.egov.usda.gov/

Spahni, R., Wania, R., Neef, L., van Weele, M., Pison, I., Bousquet, P., Frankenberg, C., Foster, P. N., Joos, F., Prentice, I. C., & van Velthoven, P. (2011). Constraining global methane emissions and uptake by ecosystems. *Biogeosciences*, *8*(6), 1643–1665. https://doi.org/10.5194/bg-8-1643-2011

Stanley, E. H., Casson, N. J., Christel, S. T., Crawford, J. T., Loken, L. C., & Oliver, S. K. (2015). The ecology of methane in streams and rivers: Patterns, controls, and global significance. *Ecological Monographs*. https://doi.org/10.1890/15-1027.1

Stanley, E. H., Casson, N. J., Christel, S. T., Crawford, J. T., Loken, L. C., & Oliver, S. K. (2016). The ecology of methane in streams and rivers: Patterns, controls, and global significance. *Ecological Monographs*, *86*(2), 146–171. https://doi.org/10.1890/15-1027

Tangen, B. A., & Bansal, S. (2019). Hydrologic Lag Effects on Wetland Greenhouse Gas Fluxes. *Atmosphere*, *10*(5), 269. https://doi.org/10.3390/atmos10050269

Teh, Y. A., Diem, T., Jones, S., Huaraca Quispe, L. P., Baggs, E., Morley, N., Richards, M., Smith, P., & Meir, P. (2014). Methane and nitrous oxide fluxes across an elevation gradient in the tropical Peruvian Andes. *Biogeosciences*, *11*(8), 2325–2339. https://doi.org/10.5194/bg-11-2325-2014

Thornton, B. F., Wik, M., & Crill, P. M. (2016). Double-counting challenges the accuracy of high-latitude methane inventories: DOUBLE-COUNTING ARCTIC METHANE. *Geophysical Research Letters*, *43*(24), 12,569-12,577. https://doi.org/10.1002/2016GL071772

Tranvik, L. J., Downing, J. A., Cotner, J. B., Loiselle, S. A., Striegl, R. G., Ballatore, T. J., Dillon, P., Finlay, K., Fortino, K., Knoll, L. B., Kortelainen, P. L., Kutser, T., Larsen, Soren., Laurion, I., Leech, D. M., McCallister, S. L., McKnight, D. M., Melack, J. M., Overholt, E., … Weyhenmeyer, G. A. (2009). Lakes and reservoirs as regulators of carbon cycling and climate. *Limnology and Oceanography*, *54*(6part2), 2298–2314. https://doi.org/10.4319/lo.2009.54.6_part_2.2298

Treat, C. C., Bloom, A. A., & Marushchak, M. E. (2018). Non-growing season methane emissions are a significant component of annual emissions across northern ecosystems. *Global Change Biology*. https://doi.org/10.1111/gcb.14137

Treby, S., Carnell, P. E., Trevathan-Tackett, S. M., Bonetti, G., & Macreadie, P. I. (2020). Assessing passive rehabilitation for carbon gains in rain-filled agricultural wetlands. *Journal of Environmental Management*, *256*, 109971. https://doi.org/10.1016/j.jenvman.2019.109971

Tucker, C. J. (1979). Red and photographic infrared linear combinations for monitoring vegetation. *Remote Sensing of Environment*, *8*(2), 127–150. https://doi.org/10.1016/0034-4257(79)90013-0

Turetsky, M. R., Kotowska, A., Bubier, J., Dise, N. B., Crill, P., Hornibrook, E. R. C., Minkkinen, K., Moore, T. R., Myers-Smith, I. H., Nykänen, H., Olefeldt, D., Rinne, J., Saarnio, S., Shurpali, N., Tuittila, E.-S., Waddington, J. M., White, J. R., Wickland, K. P., & Wilmking, M. (2014). A synthesis of methane emissions from 71 northern, temperate, and subtropical wetlands. *Global Change Biology*, *20*(7), 2183–2197. https://doi.org/10.1111/gcb.12580

U. S. Fish and Wildlife Service. (2019). *National Wetlands Inventory website*. U.S. Department of the Interior, Fish and Wildlife Service. http://www.fws.gov/wetlands/

Vanderhoof, M., Alexander, L. C., & Todd, M. J. (2016). Temporal and spatial patterns of wetland extent influence variability of surface water connectivity in the Prairie Pothole Region, United States. *Landscape Ecology*, *31*(4), 805–824. https://doi.org/10.1007/s10980-015-0290-5

Vanderhoof, M., Christensen, J., Beal, Y.-J. G., DeVries, B., Lang, M. W., Hwang, N., Mazzarella, C., & Jones, J. W. (2020). Isolating Anthropogenic Wetland Loss by Concurrently Tracking Inundation and Land Cover Disturbance

across the Mid-Atlantic Region, U.S. *Remote Sensing*, *12*(9), 1464. https://doi.org/10.3390/rs12091464

Vanderhoof, M., Distler, H. E., Lang, M. W., & Alexander, L. C. (2018). The influence of data characteristics on detecting wetland/stream surface-water connections in the Delmarva Peninsula, Maryland and Delaware. *Wetlands Ecology and Management*, *26*(1), 63–86. https://doi.org/10.1007/s11273-017-9554-y

Vanderhoof, M., Distler, H., Mendiola, D., & Lang, M. (2017). Integrating Radarsat-2, Lidar, and Worldview-3 Imagery to Maximize Detection of Forested Inundation Extent in the Delmarva Peninsula, USA. *Remote Sensing*, *9*(2), 105. https://doi.org/10.3390/rs9020105

Vanderhoof, M. K., Distler, H. E., Lang, M. W., & Alexander, L. C. (2018). The influence of data characteristics on detecting wetland/stream surface-water connections in the Delmarva Peninsula, Maryland and Delaware. *Wetlands Ecology and Management*, *26*(1), 63–86. https://doi.org/10.1007/s11273-017-9554-y

Vanderhoof, M. K., & Lang, M. (2017). *Data Release for the influence of data characteristics on detecting wetland/stream surface-water connections in the Delmarva Peninsula, Maryland and Delaware* [Data set]. U.S. Geological Survey. https://doi.org/10.5066/F70C4T8F

Vanselow-Algan, M., Schmidt, S. R., Greven, M., Fiencke, C., Kutzbach, L., & Pfeiffer, E.-M. (2015). High methane emissions dominated annual greenhouse gas balances 30 years after bog rewetting. *Biogeosciences*, *12*(14), 4361–4371. https://doi.org/10.5194/bg-12-4361-2015

Vermote, E. F., Tanre, D., Deuze, J. L., Herman, M., & Morcette, J.-J. (1997). Second Simulation of the Satellite Signal in the Solar Spectrum, 6S: An overview. *IEEE Transactions on Geoscience and Remote Sensing*, *35*(3), 675–686. https://doi.org/10.1109/36.581987

Waddington, J. M., & Day, S. M. (2007). Methane emissions from a peatland following restoration. *Journal of Geophysical Research: Biogeosciences*, *112*(G3), n/a-n/a. https://doi.org/10.1029/2007JG000400

Wania, R., Melton, J. R., Hodson, E. L., Poulter, B., Ringeval, B., Spahni, R., Bohn, T., Avis, C. A., Chen, G., Eliseev, A. V., Hopcroft, P. O., Riley, W. J., Subin, Z. M., Tian, H., Brovkin, V., van Bodegom, P. M., Kleinen, T., Yu, Z. C., Singarayer, J. S., … Kaplan, J. O. (2012). Present state of global wetland extent and wetland methane modelling: Methodology of a model intercomparison project (WETCHIMP). *Geoscientific Model Development Discussions*, *5*(4), 4071–4136. https://doi.org/10.5194/gmdd-5-4071-2012

Wania, R., Melton, J. R., Hodson, E. L., Poulter, B., Ringeval, B., Spahni, R., Bohn, T., Avis, C. A., Chen, G., Eliseev, A. V., Hopcroft, P. O., Riley, W. J., Subin, Z. M., Tian, H., van Bodegom, P. M., Kleinen, T., Yu, Z. C., Singarayer, J. S., Zürcher, S., … Kaplan, J. O. (2013). Present state of global wetland extent and wetland methane modelling: Methodology of a model inter-comparison project (WETCHIMP). *Geoscientific Model Development*, *6*(3), 617–641. https://doi.org/10.5194/gmd-6-617-2013

Webb, J. R., Santos, I. R., Maher, D. T., & Finlay, K. (2019). The Importance of Aquatic Carbon Fluxes in Net Ecosystem Carbon Budgets: A Catchment-Scale Review. *Ecosystems*, *22*(3), 508–527. https://doi.org/10.1007/s10021-018-0284-7

Winslow, L. A., Zwart, J. A., Batt, R. D., Dugan, H. A., Woolway, R. I., Corman, J. R., Hanson, P. C., & Read, J. S. (2016). LakeMetabolizer: An R package for estimating lake metabolism from free-water oxygen using diverse statistical models. *Inland Waters*, *6*(4), 622–636. https://doi.org/10.1080/IW-6.4.883

Wu, Q., Lane, C., & Liu, H. (2014). An Effective Method for Detecting Potential Woodland Vernal Pools Using High-Resolution LiDAR Data and Aerial Imagery. *Remote Sensing*, *6*(11), 11444–11467. https://doi.org/10.3390/rs61111444

Wu, Q., Lane, C. R., Wang, L., Vanderhoof, M. K., Christensen, J. R., & Liu, H. (2019). Efficient Delineation of Nested Depression Hierarchy in Digital Elevation Models for Hydrological Analysis Using Level-Set Method. *JAWRA Journal of the American Water Resources Association*, *55*(2), 354–368. https://doi.org/10.1111/1752-1688.12689

Xaypraseuth, P., Satish, R., & Chatterjee, A. (2015). NISAR spacecraft concept overview: Design challenges for a proposed flagship dual-frequency SAR mission. *2015 IEEE Aerospace Conference*, 1–11. https://doi.org/10.1109/AERO.2015.7118935

Yan, X., Yagi, K., Akiyama, H., & Akimoto, H. (2005). Statistical analysis of the major variables controlling methane emission from rice fields. *Global Change Biology*, *11*(7), 1131–1141. https://doi.org/10.1111/j.1365-2486.2005.00976.x

Yang, W. H., McNicol, G., Teh, Y. A., Estera-Molina, K., Wood, T. E., & Silver, W. L. (2017). Evaluating the Classical Versus an Emerging Conceptual Model of Peatland Methane Dynamics: Peatland Methane Dynamics. *Global Biogeochemical Cycles*, *31*(9), 1435–1453. https://doi.org/10.1002/2017GB005622

Yeo, I.-Y., Lang, M. W., Lee, S., McCarty, G. W., Sadeghi, A. M., Yetemen, O., & Huang, C. (2019). Mapping landscape-level hydrological connectivity of headwater wetlands to downstream waters: A geospatial modeling approach - Part 1. *Science of The Total Environment*, *653*, 1546–1556. https://doi.org/10.1016/j.scitotenv.2018.11.238

Zeileis, A., Fisher, J. C., Hornik, K., Ihaka, R., McWhite, C. D., Murrell, P., Stauffer, R., & Wilke, C. O. (2019). colorspace: A Toolbox for Manipulating and Assessing Colors and Palettes. *ArXiv:1903.06490 [Cs, Stat]*. http://arxiv.org/abs/1903.06490

Zhang, Z., Zimmermann, N. E., Kaplan, J. O., & Poulter, B. (2016). Modeling spatiotemporal dynamics of global wetlands: Comprehensive evaluation of a new sub-grid TOPMODEL parameterization and uncertainties. *Biogeosciences*, *13*(5), 1387–1408. https://doi.org/10.5194/bg-13-1387-2016